Uranium(III) and uranium(IV) *meta*-terphenyl thiolate complexes

Benjamin L. L. Réant,[1,2] John A. Seed,[1,2] George F. S. Whitehead,[2] and Conrad A. P. Goodwin*[1,2]

[1] Centre for Radiochemistry Research, The University of Manchester, Oxford Road, Manchester, M13 9PL (UK).

[2] Department of Chemistry, The University of Manchester, Oxford Road, Manchester, M13 9PL (UK).

*Correspondence: *conrad.goodwin@manchester.ac.uk*

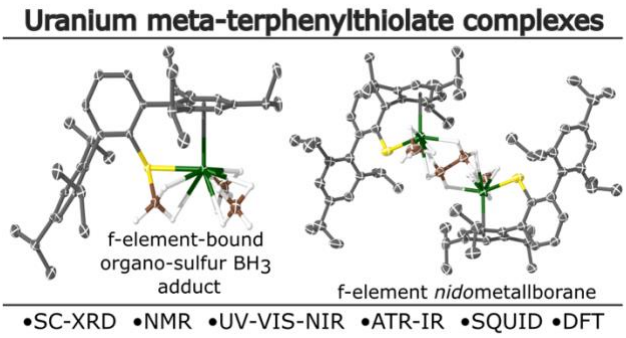

Abstract

We report the synthesis and characterization of crystalline uranium(IV) and uranium(III) complexes supported by the bulky hexa-*iso*-propyl-*m*-terphenylthiolate ligand system, SAr^{iPr6} (SAr^{iPr6} = {SC_6H_3-2,6-$(Tripp)_2$}; Tripp = 2,4,6-*i*Pr-C_6H_2). These constitute the first examples of *m*-terphenylthiolate complexes of uranium in any oxidation state and highlight the supporting role of U···arene interactions in the isolation of heteroleptic complexes with this ligand set, and demonstrate the diverse reactivity of $[U^{IV}(BH_4)_4]$. Treatment of $U^{IV}Cl_4$ with two equivalents of $KSAr^{iPr6}$ in Et_2O afforded $[U^{IV}(SAr^{iPr6})_2(Cl)_2]$ (**1**) in poor yield along with several crystals of the Et_2O adduct, $[U^{IV}(SAr^{iPr6})_2(Cl)_2(Et_2O)_2]$ (**1·Et₂O**). While the reaction between $[U^{IV}(BH_4)_4]$ and one equivalent of $KSAr^{iPr6}$ in toluene gave several crystals of the poorly soluble double salt, $[U^{IV}(\mu\text{-}SAr^{iPr6})(BH_4)_2(\mu\text{-}BH_4)(\mu^3\text{-}BH_4)K]_2$ (**2**), exposing the crude reaction mixture to Et_2O gave the oxidized disulfide ligand dimer, $(SAr^{iPr6})_2$ as the sole identifiable product. The reaction between $[U^{IV}(BH_4)_4]$ and one equivalent of $HSAr^{iPr6}$ in hot toluene gave $[U^{III}(H_3B{\cdot}SAr^{iPr6}\ \kappa S,H,H)(BH_4)_2]$ (**3**) – the net product of thermolytic reduction of the uranium and deprotonation of the arylthiol. Complex **3** proved resistant to further substitution using either $HSAr^{iPr6}$ or $KSAr^{iPr6}$. Both U(III) mono-arylthiolates, $[U^{III}(SAr^{iPr6})(BH_4)_2]$ (**4a**) and $[\{U^{III}(SAr^{iPr6})(BH_4)\}_2\{\mu\text{-}B_2H_6\}]$ (**4b**) were isolated as a mixture from the reaction between $[U^{III}(BH_3)_3(toluene)]$ and one equivalent of $KSAr^{iPr6}$. Complex **4b** is a rare example of a *nido*-mettaloborane. When two equivalents of $KSAr^{iPr6}$ were reacted with $[U^{III}(BH_3)_3(toluene)]$, the *bis*-arylthiolate complex $[U^{III}(SAr^{iPr6})_2(BH_4)]$ (**5**) was isolated in good yield. Complexes **1**–**5** have been characterized variously by single-crystal X-ray diffraction, multi-nuclear NMR spectroscopy, infra-red spectroscopy, UV-Vis-NIR spectroscopy, SQUID magnetometry, elemental analyses as appropriate. Quantum chemical calculations have been employed to interpret the nature of the U–S bonding interactions across these U(III) and U(IV) complexes.

Introduction

The coordination chemistry of uranium (U) with ligands featuring hard first-row donors such as amides and alkoxides (along with their aryl congeners) in oxidation states from III–VI is a mature area.[1-6] Soft sulfur-based extractants are crucial in minor actinide separation processes, and so the chemistry of U–S bonded species is of great importance.[7-12] However, the molecular coordination chemistry of U(III) and U(IV) with thiolates and arylthiolates is underdeveloped relative to first-row congeners. Reported routes to U–S bonded species include protonolysis,[13-15] salt-elimination,[14,16-18] σ-bond metathesis,[19-21] or oxidation of lower oxidation state uranium precursors.[22-28] Generally, structurally characterized examples of uranium(III) with sulfur donors are rarer than with higher oxidation states such as U(IV).[29]

Advances in low oxidation state (M(IV) and below) uranium chemistry have shown that U(II) is accessible within cyclopentadienyl (Cp) ligand frameworks,[30-32] and also using hard aryloxide and anilide ligands where metal-to-ligand back-bonding affords δ-bonding interactions which reduce charge build-up on the metal.[33-35] Softer sulfur-based ligands may also stabilize uranium in lower oxidation states such as U(III) or U(II) with different properties and reactivities to those using harder donors due to the potential for increased M–L covalency, but there is a paucity of suitable precursor complexes with which to explore this. It would be instructive to advance low oxidation state uranium chemistry beyond first-row donors to explore the effect of softer donor systems on the electronic structure of these rare ions.[36,37] Given the stability imparted by δ-bonding interactions, and our own interest in *f*-block arene bonding,[38,39] we were inspired by Meyer's recent work on a U(III) complex featuring a tethered *tris*-arylthiolate ligand system (**Figure 1A**), and sought other frameworks which provide both a sulfur donor and pendant arene groups to facilitate U→arene backdonation and therefore possibly stabilize lower formal oxidation states of uranium.[40]

Both Niemeyer, and more recently Evans,[41] have previously shown that Power's *m*-terphenyl ligand, {SAr$^{i\text{Pr6}}$} (SAr$^{i\text{Pr6}}$ = {SC$_6$H$_3$-2,6-(Tripp)$_2$}; Tripp = 2,4,6-*i*Pr-C$_6$H$_2$),[42,43] supports lanthanide (Ln) aryl thiolate complexes with metal–arene interactions in both the Ln(III) and Ln(II) oxidation states (**Figure 1B**). This framework is structurally analogous to that used in Odom and Boncella's arene-stabilized U(II) complex, [U^{II}(NHAr$^{i\text{Pr6}}$)$_2$],[35] and also recently reported M(II) rare-earth complexes by Odom and Demir, and some of us (**Figure 1C**).[39,44]

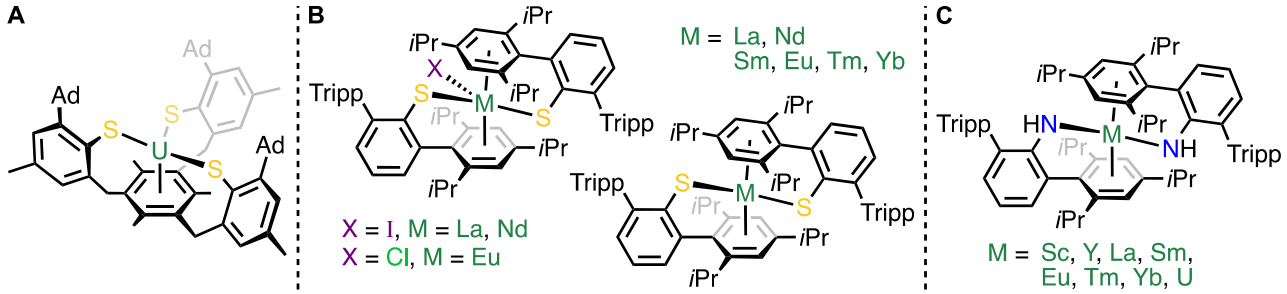

Figure 1. (A) Meyer's U(III) tethered *tris*-arylthiolate complex, complex **A**; (B) a heteroleptic Eu(III) arylthiolate complex along with Ln(II) congeners; (C) neutral M(II) terphenyl-anilide complexes.

Here, progress towards the isolation of low oxidation state uranium arylthiolates is reported, which encompass a range of heteroleptic U(IV) and U(III) structures, and which can be accessed from [U^{IV}(BH$_4$)$_4$] by salt elimination, protonolysis, and thermolysis routes. These complexes have been variously characterized by single-crystal X-ray diffraction, multi-nuclear NMR, ATR-IR, and UV-Vis-NIR spectroscopies, SQUID magnetometry, and elemental analyses as appropriate. Quantum chemical calculations have been used to examine the U–S interactions.

Results and Discussion

Synthesis

As both U(IV) and U(III) arylthiolate complexes were sought, we first explored $U^{IV}Cl_4$ as a precursor in salt elimination reactions, reasoning that U(III) complexes might be subsequently accessed through reduction. Stirring two equivalents of $KSAr^{iPr6}$ with $U^{IV}Cl_4$ in Et_2O led to the precipitation of a red powder and gave a pale amber solution. Workup and crystallization of the red powder from hot *n*-hexane gave $[U^{IV}(SAr^{iPr6})_2(Cl)_2]$ (**1**) in low crystalline yield (20%; **Scheme 1**) which gave satisfactory results by elemental microanalysis. The ^{1}H NMR spectrum of **1** in d_6-benzene shows broad resonances at δ_H = 16.85 ($\bar{\upsilon}$ = 195 Hz, *i*Pr C*H*$_3$) and –1.00 ($\bar{\upsilon}$ = 133 Hz, *i*Pr C*H*), along with a sharper singlet at 10.60 ppm (Tripp C*H*), which were tentatively assigned by their relative integrals. The SAr 3,4,5-C*H* groups could not be conclusively located. The pale amber Et_2O supernatant contained unreacted $KSAr^{iPr6}$. The use of toluene as the reaction medium or extended reaction times reproducibly resulted in the isolation of unreacted $KSAr^{iPr6}$. On one attempt, several crystals of $[U^{IV}(SAr^{iPr6})_2(Cl)_2(OEt_2)_2]$ (**1·Et$_2$O**) were isolated as a co-crystallized mixture with unreacted $KSAr^{iPr6}$. Attempts to isolate the diamagnetic Th(IV) analogue were unsuccessful using $[Th^{IV}Cl_4(DME)_2]$,[45] resulting in the conversion of $KSAr^{iPr6}$ to $HSAr^{iPr6}$ along with unknown Th-containing byproducts (**Scheme 1**).

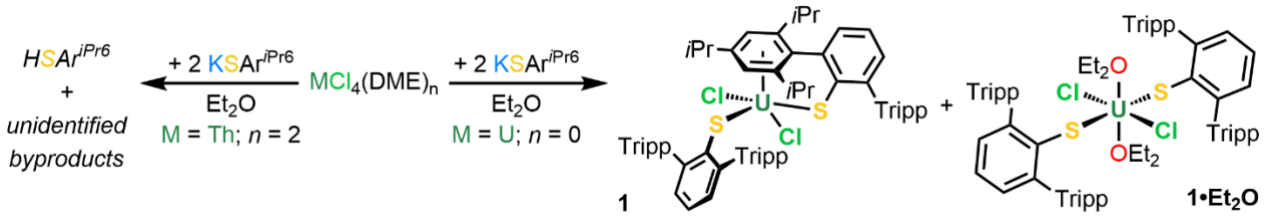

Scheme 1. The synthesis of $[U^{IV}(SAr^{iPr6})_2(Cl)_2]$ (**1**) from $U^{IV}Cl_4$ and two equivalents of $KSAr^{iPr6}$ in Et_2O, and attempted synthesis of the Th(IV) analogue from $[ThCl_4(DME)_2]$. Tripp = {C_6H_2-2,4,6-*i*Pr$_3$}.

Given the sensitivity to solvent choice, sluggish reactions, and low yield of **1** from $U^{IV}Cl_4$,[46] an alternative U(IV) precursor was sought. Daly recently reported the convenient synthesis of $[U^{IV}(BH_4)_4]_n$ by ball-milling $U^{IV}Cl_4$ and $LiBH_4$.[47] This is a useful precursor as (i) the synthesis does not require U-metal, unlike $[UI_4(OEt_2)_2]$;[48,49] (ii) the $\{BH_4\}$ group is synthetically versatile;[50-57] and, (iii) careful thermolysis of $[U^{IV}(BH_4)_4]_n$ gives U(III)-borohydrides (**Scheme 2A**) which Ephritikhine has shown can be isolated as U(III) arene adducts such as $[U^{III}(BH_4)_3(toluene)]$, therefore allowing the same material to be employed in both U(IV) and U(III) chemistry.[58]

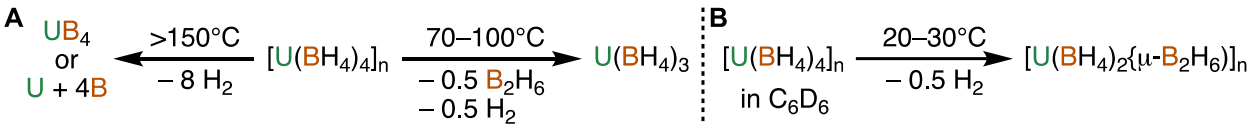

Scheme 2. (A + B) Different pathways for the thermolysis of $[U^{IV}(BH_4)_4]_n$ depending on the reaction conditions.

Two different crystalline phases of $[U^{IV}(BH_4)_4]_n$ can be obtained depending on the temperature of the condensing surface during the sublimation step.[59-63] $[U^{IV}(BH_4)_4]_n$-α forms when the condensation surface is *ca*. 20°C, has rather poor solubility in ethereal solvents (<20 $g \cdot L^{-1}$ in Et_2O),[64] and produces large dark green/black block-like crystals on the surface of the sublimator (see the *Supporting Information* for images). $[U^{IV}(BH_4)_4]_n$-β forms when the condensing surface is at –80°C, has a much higher solubility in organic solvents (up to 44 $g \cdot L^{-1}$ in benzene),[62,63] and takes on a paler green/brown color. Herein, we have used both phases without a discernible difference in their reactivities. When a portion of dark green/black crystalline $[U^{IV}(BH_4)_4]_n$-α was left standing in d_6-benzene at room temperature for 7 days, several dark red crystals deposited and were shown to be $[U^{IV}(BH_4)_2\{\mu\text{-}B_2H_6\}]_n$ by SC-XRD (**Scheme 2B**, and see *Supporting Information* for the molecular structure). No further analysis could be obtained on this material, which was consumed during the SC-

XRD study. However, subsequent examination of $[U^{IV}(BH_4)_4]_n$-β in d_6-benzene (δ_H = 134.84, br. singlet, $h_{1/2}$ = 556 Hz; δ_B = 130.86, quintet $^1J_{BH}$ = 87.0 Hz)[47,60,61,65] by ^{1}H NMR spectroscopy shows that it slowly liberates H_2 (as evidenced by a peak at δ_H = 4.47 ppm) at room temperature, and this is accompanied by the growth of a broad singlet at δ_B = 31.10, and a complex feature at δ_B = 17.29 which we suggest is due to the formation of a small quantity of $[U^{IV}(BH_4)_2\{\mu\text{-}B_2H_6\}]_n$.

Using the $[U^{IV}(BH_4)_4]_n$ precursor, mono-substituted U(IV) SAr^{iPr6} complexes were targeted first to examine whether reduced steric saturation would facilitate the isolation of crystalline material. The reaction between $[U^{IV}(BH_4)_4]_n$ and one equivalent of KSAr^{iPr6} in toluene gave a single crop of the double salt $[U^{IV}(\mu\text{-}SAr^{iPr6})(BH_4)_2(\mu\text{-}BH_4)(\mu^3\text{-}BH_4)K]_2$ (**2**) as red crystals from hot toluene in very poor crystalline yield as the solvent cooled (3% isolated crystalline yield; **Scheme 3**). A batch of **2** was isolated (in 26% yield) by repeating the reaction and washing the precipitated solids with toluene. The ATR-IR spectrum of this material was found to be superposable with that of crystalline **2**. A large number of poorly resolved features between ν = 2,500 and 2,000 cm^{-1} suggest a range of binding modes for the {BH_4} groups.[66] The ^{1}H NMR spectrum of **2** in d_6-benzene shows seven broad peaks spanning δ_H = 14.46 to –4.54, commensurate with C_2 symmetry in solution and both Tripp groups being equivalent on the NMR timescale. A further 12 minor ^{1}H resonances were observed outside of this range between 87.15 and –76.69 ppm, which we tentatively attribute to the various B*H* environments. The ^{11}B NMR spectrum shows one single resonance at δ_B = 141.25, which is similar to $[U^{IV}(BH_4)_4]_n$ (δ_B = 131.6). An attempt to extract crude **2** into Et_2O (instead of toluene) gave the sulfide-bridged dimer $(SAr^{iPr6})_2$ as the only isolable crystalline product (**Scheme 3**).

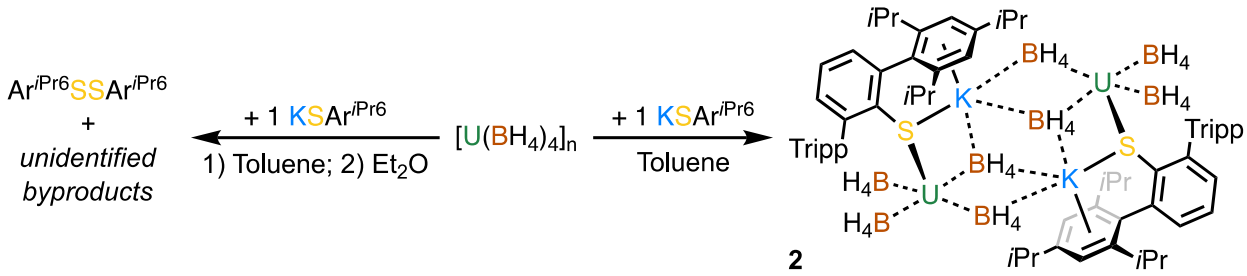

Scheme 3. The synthesis of $[U^{IV}(\mu\text{-}SAr^{iPr6})(BH_4)_2(\mu\text{-}BH_4)(\mu^3\text{-}BH_4)K]_2$ (**2**) from $[U^{IV}(BH_4)_4]_n$ and one equivalent of $KSAr^{iPr6}$ in toluene.

Protonolysis was explored as an alternative route to mono-arylthiolate U(IV) complexes through the reaction of $[U^{IV}(BH_4)_4]_n$ with one equivalent of $HSAr^{iPr6}$ in hot toluene (**Scheme 4**). After workup, this gave red-green crystals of $[U^{III}(H_3B{\cdot}SAr^{iPr6}\ \kappa S,H,H)(BH_4)_2]$ (**3**) in good yield (69%). Complex **3** is the net product of thermolytic reduction of $[U^{IV}(BH_4)_4]_n$, deprotonation of $HSAr^{iPr6}$, and capture of byproduct BH_3 by the S-atom lone pair. Doublets at ν = 2,467 and 2,152 cm^{-1} in the ATR-IR spectrum of **3** are attributed to stretching modes from B–H_t (A_1) {κ^2-$H_3B{\cdot}SAr^{iPr6}$} and B–H_b (A_1 and E) from {κ^3-BH_4} respectively.[66] The ^{1}H NMR spectrum of **3** in d_6-benzene could not be definitively assigned. The absence of residual $HSAr^{iPr6}$ and satisfactory elemental microanalysis results suggest the large number of peaks is due to low symmetry in solution. It has been shown that M···Tripp contacts can be sufficiently strong to preclude the exchange of the metal-bound and "terminal" Tripp groups in $[Yb(NHAr^{iPr6})_2]$,[39] and this may be the case for **3**. The ^{11}B NMR spectrum in d_6-benzene revealed three broad singlets (δ_B = 102.91, 75.24, 59.01). By comparison with **4a**/**4b** (see below), the resonance at 59.01 ppm can be assigned to the B-atom of the {κ^2-$H_3\underline{B}{\cdot}SAr^{iPr6}$} ligand. The remaining two peaks in the spectrum of **3** cannot be definitely assigned, but their similarity to features seen in **4a**/**4b** suggests a mixture of {κ^3-BH_4}, and also {μ-B_2H_6}$^{2-}$ groups are present, the latter of which may arise due to dehydrocoupling in solution.[67-69] The ^{11}B NMR spectrum of $[U^{III}(BH_4)_3(THF)_2]$ shows a broad singlet at a significantly different chemical shift (d_6-benzene, δ_B = 153;[47] d_8-THF, δ_B = 230)[57] to either

of the remaining features and so we have discounted the presence of residual U(III) precursor.

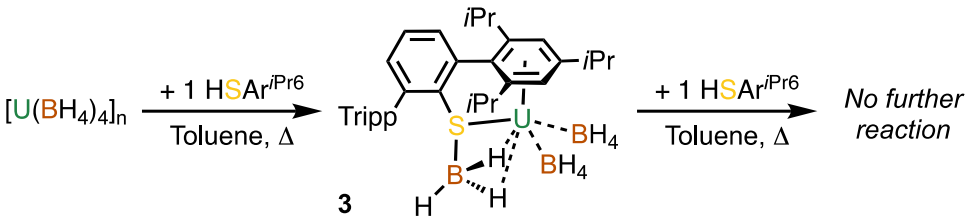

Scheme 4. The synthesis of $[U^{III}(H_3B{\cdot}SAr^{iPr6}\text{-}\kappa S,H,H)(BH_4)_2]$ (**3**) from $[U^{IV}(BH_4)_4]$ and one equivalent of $HSAr^{iPr6}$ in toluene.

Given the facile thermolytic reduction of U(IV) to U(III) under the conditions above, we instead sought to isolate mono-arylthiolate complexes using a pre-formed U(III) precursor and a salt-elimination strategy. $[U^{IV}(BH_4)_4]_n$ was thermolyzed in toluene and dried under vacuum to give $[U^{III}(BH_4)_3(toluene)]$ as a red microcrystalline powder which was used *in situ* without further purification.[47,58] Addition of Et_2O to a pre-cooled (–98 °C) mixture of $[U^{III}(BH_4)_3(toluene)]$ and one equivalent of $KSAr^{iPr6}$ gave, after workup and crystallization from *n*-hexane, dark red crystals of $[U^{III}(SAr^{iPr6})(BH_4)_2]$ (**4a**). A second crystalline crop was isolated from *n*-hexane after trituration with hot toluene, and was found to be dimeric $[\{U^{III}(SAr^{iPr6})(BH_4)\}_2(\mu\text{-}B_2H_6)]$ (**4b**) – see **Scheme 5**. The combined yield was fair (37%), and the ATR-IR spectra from each crop are almost perfectly superposable, suggesting both batches contain a mixture of **4a** and **4b** in roughly equal proportions. These spectra show a strong singlet at ν = 2,472 cm^{-1} for the $\{\kappa^3\text{-}BH_4\}$ B–H_t A_1 stretching mode, which presents with poorly-resolved doublet character (Δ *ca*. 25 cm^{-1}) in some batches, suggesting the presence of a $\{\kappa^2\text{-}BH_4\}$ coordination mode. A doublet at 2,154 cm^{-1} (Δ *ca*. 60 cm^{-1}) likely arises from the A_1 and E bridging B–H_b stretching modes of the $\{\kappa^3\text{-}BH_4\}$ groups.[66] These first two sets of peaks are essentially identical to those found in **3**, which aided assignment. Notably, the spectra for **4a**/**4b** have an additional feature at ν = 2,281 cm^{-1} (singlet) which is

absent in **3**, and is similar to other *nido*-metalloborane complexes with reported IR data,[70-74] and which we tentatively assign to the κ^2-BH_3 stretching mode of the $\{\mu\text{-}B_2H_6\}^{2-}$ moiety. ^{1}H NMR spectra of the **4a** and **4b** mixture could not be assigned conclusively. Still, two singlet resonances (δ_B = 102.89, 75.42) were observed in the ^{11}B NMR spectrum of the mixture, which are remarkably similar to those observed for complex **3**. We tentatively assign these to the terminal $\{\kappa^3\text{-}BH_4\}$ and $\{\mu\text{-}B_2H_6\}^{2-}$ groups in **4a**/**4b**. A weak feature at *ca*. δ_B = 60 is likely be due to traces of $\{\kappa^2\text{-}H_3\underline{B}\cdot SAr^{iPr6}\}$ by analogy to **3**. Attempts to monitor the thermal conversion of **4a** to **4b** by ^{1}H and ^{11}B NMR spectroscopy were inconclusive (see *Supporting Information*).

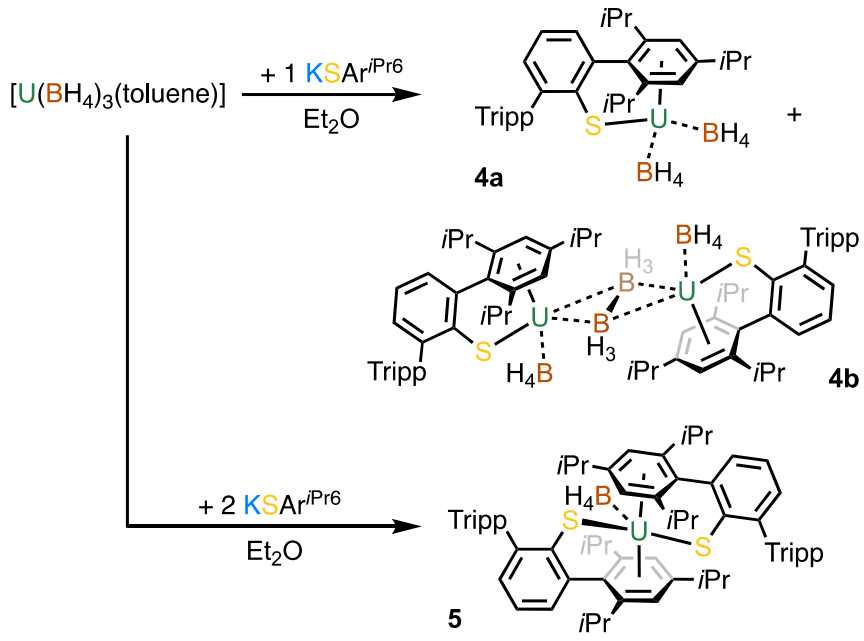

Scheme 5. The synthesis of both $[U^{III}(SAr^{iPr6})(BH_4)_2]$ (**4a**) and $[\{U^{III}(SAr^{iPr6})(BH_4)\}_2(\mu\text{-}B_2H_6)]$ (**4b**) from $[U^{III}(BH_4)_3(toluene)]$ and one equivalent of $KSAr^{iPr6}$ in Et_2O; and $[U^{III}(SAr^{iPr6})_2(BH_4)]$ (**5**) from $[U^{III}(BH_4)_3(toluene)]$ and two equivalents of $KSAr^{iPr6}$.

With a range of mono-arylthiolate complexes in hand which demonstrate the ability of this ligand set to support both U(III) and U(IV)-arene interactions, the synthesis of $[U^{III}(SAr^{iPr6})_2(BH_4)]$ (**5**) was attempted by reacting two equivalents of $KSAr^{iPr6}$ with

$[U^{III}(BH_4)_3(toluene)]$ in Et_2O (**Scheme 5**). Crystallization from hot hexane gave **5** in modest yield (52%). The ATR-IR spectrum of microcrystalline **5** shows a distorted doublet (ν = 2,480 cm^{-1}, A_1 and B_1) and a singlet (ν = 2,134 cm^{-1}, A_1 and B_2) for the B–H stretching modes, commensurate with a $\{\kappa^2\text{-}BH_4\}$ group. The ^{1}H NMR spectrum of **5** in d_6-benzene displayed broadened resonances between δ_H = 8 to –1 for the $\{SAr^{iPr6}\}$ ligand which integrate well for a C_2 symmetric structure in solution whereby the metal-bound and terminal Tripp groups exchange on the NMR timescale, though definitive assignment has not been possible. The $\{BH_4\}$ group appears at δ_H = 126.58 in the ^{1}H NMR spectrum, which is shifted from both $[U^{IV}(BH_4)_4]$ (δ_H = 130.86) and $[U^{III}(BH_4)_3(THF)_2]$ (δ_H = 118.58). A broad resonance for the $\{\kappa^2\text{-}BH_4\}$ group is observed in the ^{11}B spectrum at δ_B = 177.75 (FWHM = 340 Hz).

Molecular structures

The molecular structures of complexes **1**, **1·Et₂O**, and **2**–**5** were determined by single crystal X-ray diffraction (SC-XRD) studies, and selected bond metrics are given in **Table 1**. Complexes **1** and **1·Et₂O**, crystallized from hexane and toluene respectively in the $P\bar{1}$ space group (see **Figure 2** for the molecular structure of **1·Et₂O**, and the *Supporting Information* for **1**). In the case of **1**, the resolution of the data is limited due to weak diffraction at higher angles due to the large unit cell (V = 50,235 Å^3; Z' = 10). While the connectivity is unambiguous and supported by further characterization data, there is limited precision associated with the metrical parameters. However, the large number of molecular units allows us to provide mean bond lengths and angles (where the number in parenthesis is the standard deviation of the mean, rather than the crystallographic ESD) for the U–S (2.675(5) Å) and U–Cl (2.545(23) Å) distances, and also the S–U–S and Cl–U–Cl angles (154.5(7)° and 95.6(5)° respectively). The geometry is best described as *pseudo*-sawhorse with respect to the U, Cl and S-atoms, while the U-center is capped by a single η^6-Tripp group

for each molecule (mean U···η^6-Tripp = 2.591(2) Å). On the other hand, complex **1·Et$_2$O** which is an Et$_2$O adduct of **1**, is octahedral (*SHAPE* analysis = 0.306)[75] and has an inversion center situated at the U-atom. The U–Cl (2.5699(10) Å) bond lengths are indistinguishable at the 3σ-level of statistical significance from the mean in **1**, and the U–S (2.6526(9) Å) is shorter than the mean in **1** (Δ = 0.022 Å). In both **1** and **1·Et$_2$O** the U–S distances are somewhat shorter than the sum of the covalent radii for a U–S single bond (2.73 Å),[76] and is in the middle of the range of terminally bound organo-sulfur U(IV) distances reported in the CCDC (2.61(5) to 3.029(4) Å).[77-79] The U–S–C$_{ipso}$ angle (158.71(14)°) in **1·Et$_2$O** is larger than either mean values in complex **1** (115.3(5) and 123.3(6)°).

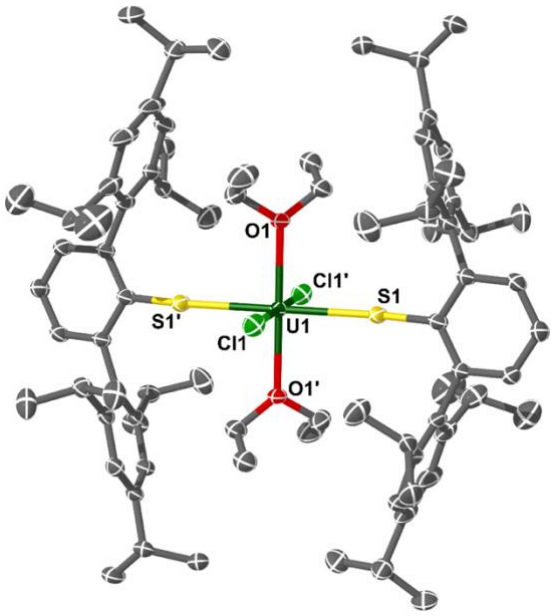

Figure 2. Molecular structure of complex **1·Et$_2$O**. Ellipsoids set at 50% probability and H-atoms removed for clarity (operations: 1–X, 1–Y, 1–Z). Selected bond lengths and angles: U1–S1 = 2.6526(9) Å, U1–Cl1 = 2.5699(10) Å, U1–O1 = 2.368(2) Å, U1–S1–C$_{ipso}$ = 158.71(14)°.

Complex **2** crystallized as a centrosymmetric dimer (*Z′* = 0.5) comprised of two {U^{IV}(BH$_4$)$_4$KSAr^{iPr6}} units, and is best described as a double salt of [U^{IV}(BH$_4$)$_4$] and [KSAr^{iPr6}] – see **Figure 3**. Each S-atom bridges between a U and a K (U–S = 2.6948(10) Å and K–S

= 3.1109(13) Å). The U–S bond of is slightly longer than in **1** and **1·Et$_2$O**, but is shorter than the sum of the covalent radii for a single bond, again implying a polar-covalent bond.[76] The K–S bond is *ca.* 0.07 Å longer than in [KSAr$^{i\text{Pr}6}$]$_2$ as a result of coordination to U(IV).[80] Complex **2** possesses {κ^3-BH$_4$} units that bind in a terminal fashion (U···B$_{BH4}$ = 2.489(6) and 2.508(7) Å), and also two different bridging modes: one μ:κ^3:κ^3 to both the U and K-atoms (U···B = 2.557(6) Å) whereas the other binds μ^3:κ^2:κ^2:κ^2 to one U-atom (U···B = 2.865(7) Å), and both K-atoms of the dimer – in all cases these distances compare well to previous structural determinations of parent [U^{IV}(BH$_4$)$_4$]$_n$,[59-63] and other U(IV)-borohydride complexes.[56,81-103] Unlike complex **1**, there are no η^6-Tripp–U interactions in **2**; instead, the softer K-atom binds to an η^6-Tripp group (η^6-Tripp$_{centroid}$···K = 2.881(2) Å).

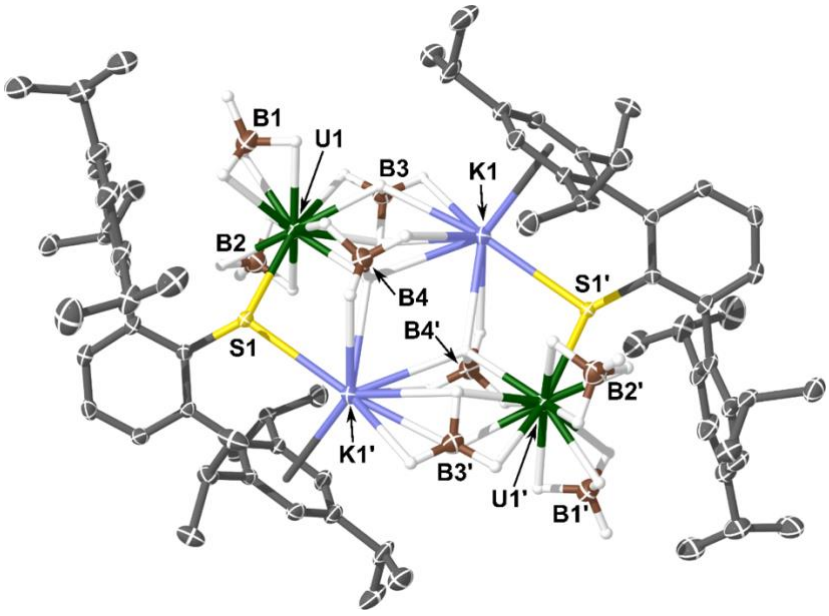

Figure 3. Molecular structure of complex **2**. Ellipsoids set at 50% probability and non-BH$_4$ H-atoms removed for clarity (operations: 1–X, 1–Y, 1–Z). Selected bond lengths and angles: U1–S1 = 2.6948(10) Å, K1–S1 = 3.1109(13) Å, U1···B1 = 2.489(6) Å, U1···B2 = 2.508(7) Å, U1···B3 = 2.557(6) Å, U1···B4 = 2.865(7) Å, K1···Tripp$_{centroid}$ = 2.881(2) Å, U1–S1–K1 = 101.94(3)°, U1–S1–C$_{ipso}$ = 124.88(14)°.

The molecular structures of the U(III) complexes **3** and **4a** are shown together in **Figure 4** (*Z*′ = 1 for both). The U–S bond in **3** (2.8824(9) Å) is elongated compared to **4a** (2.687(4) Å; Δ = 0.195(4) Å), and more so than expected from increasing the coordination number at U(IV) (*e.g.* 6-coordinate = 0.89 Å to 8-cordinate = 1.00 Å; Δ = 0.11 Å).[104] The coordination of Lewis-acidic BH_3 reduces the charge density of the S-anion, weakening the U–S interaction and so the U–S distance in **3** is one of the longest for any anionic S-donor to uranium. The U–S in complex **4a** is short compared to other U(III) thiolate complexes. For example, the range of U–S distances in $[U^{III}(SMes^*)_3]$ (Mes* = {2,4,6-*t*Bu_3-C_6H_2}) is 2.7127(11) to 2.7247(10) Å; and in Meyer's complex **A**, the three equivalent U–S distances are 2.7082(7) Å – all of which are longer by a statistically significant amount.[14,15] To the best of our knowledge, complex **4a** has the shortest U–S bond length for any structurally authenticated molecular U(III) complex, and this is likely a reflection of its electron-poor U-center.[79] While U···B distances in **3** (2.584(6) and 2.603(7) Å) and **4a** (2.56(2) and 2.56(3) Å) are statistically indistinguishable, the U···$Tripp_{centroid}$ distances (**3**, 2.5379(15) Å; **4**, 2.482(7) Å) differ by only 0.056(7) Å. These differences suggest that the change in U–S bond length is due to more than just a change in formal coordination number. The S–B bond length in complex **3** (1.939(5) Å) is within the range (1.897(8) to 2.00(2) Å) of the few previously reported complexes containing metal-bound organo-sulfur BH_3 adducts,[105-111] and to the best of our knowledge is the first example with an *f*-element.

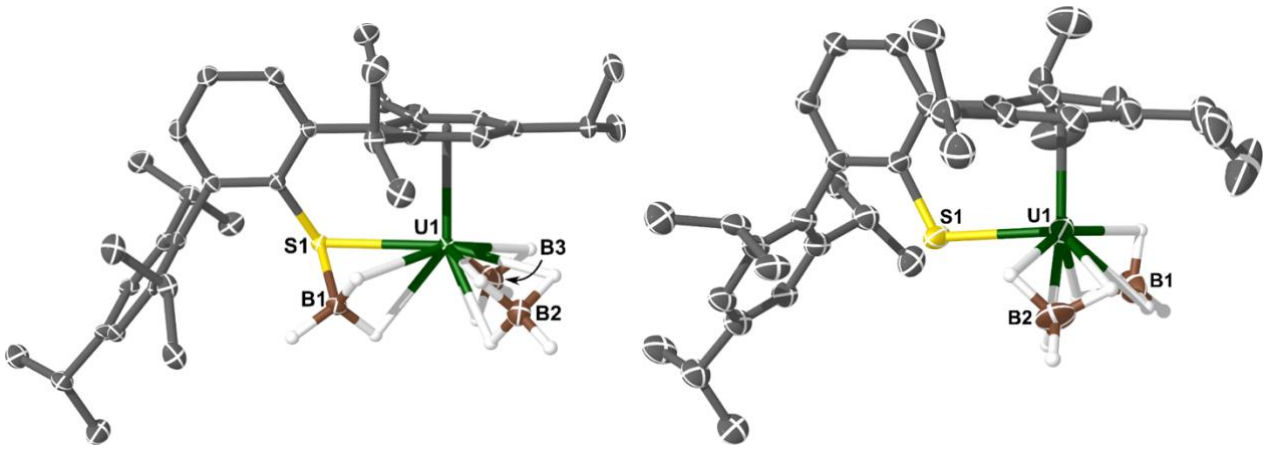

Figure 4. Molecular structure of complexes **3** (left) and **4a** (right). Ellipsoids set at 50% (**3**) and 30% (**4a**) probability, and non-BH_4 H-atoms and lattice solvent molecules removed for clarity (operations for **3** and **4a**: X, Y, Z). Selected bond lengths and angles for complex **3**: U1–S1 = 2.8824(9) Å, S1–B1 = 1.939(5) Å, U1···B2 = 2.603(7) Å, U1···B3 = 2.584(6) Å, U1···$Tripp_{centroid}$ = 2.5379(15) Å, U1–S1–B1 = 64.55(14)°, U1–S1–C_{ipso} = 109.54(12)°; complex **4a**: U1–S1 = 2.687(4) Å, U1···B1 = 2.56(2) Å, U1···B2 = 2.56(3) Å, U1···$Tripp_{centroid}$ = 2.482(7) Å, U1–S1–C_{ipso} = 113.6(5)°.

Complex **4b** (shown in **Figure 5**) crystallized as a dimer (*Z′* = 0.5) where two $\{U^{III}(SAr^{iPr6})(BH_4)\}$ units are bridged by a diborane(6) dianion, $\{B_2H_6\}^{2-}$. This structure type is equivalent to *arachno*-tetraborane(10) (B_4H_{10}) wherein two of the $\{BH_2\}$ units have been replaced by U(III)-centers, and so **4b** is the first example of an *f*-element *nido*-metalloborane (aside from $[U^{IV}(BH_4)_2\{\mu\text{-}B_2H_6\}]_n$ shown above).[112] The $\{\mu\text{-}B_2H_6\}^{2-}$ binds asymmetrically to each U-atom (U···B = 2.609(6) and 2.892(6) Å). The B–B bond length of 1.783(12) Å is within the range (1.63(3) to 1.846(4) Å)[69,113,114] of reported transition metal examples in the CCDC.[79] The U···B_{BH4} distances (2.556(8) Å) in **4b** are indistinguishable from those in **4a**. The $\{SAr^{iPr6}\}$ ligand in **4b** is disordered over two components in a 82:18 ratio, giving two U–S bond lengths (2.721(3) and 2.663(17) Å respectively).

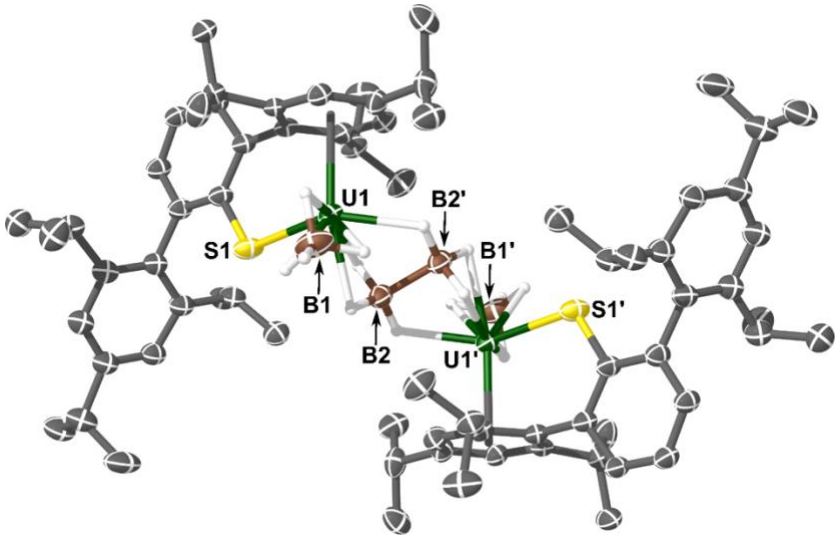

Figure 5. Molecular structure of complex **4b**. Ellipsoids set at 30% probability and non-BH_4 H-atoms removed for clarity (operations: 1–X, 1–Y, 1–Z). Selected bond lengths and angles: U1–S1 = 2.721(3) Å, U1···B1 = 2.556(8) Å, U1···B2 = 2.609(6) Å, U1···B2′ = 2.892(6) Å, U1···$Tripp_{centroid}$ = 2.5168(19) Å, U1–S1–C_{ipso} = 111.7(4)°.

The molecular structure of complex **5** (**Figure 6**) shows the U-atom is sandwiched equally between two Tripp arene rings (U···$Tripp_{centroid}$ = 2.744(1) and 2.747(2) Å) and almost perfectly within the S_2B plane (deviation = 0.004(2), below statistical significance). Despite this, **5** does not possess crystallographic C_2 symmetry (Z' = 1), and the two U–S bonds are distinct (2.7888(8) and 2.7969(7) Å; Δ = 0.0081(10) Å). The U–S lengths in **5** are longer than in both U(IV) complexes **1** and **2**, and also U(III) **4a** and **4b**, whereas those of complex **3** (2.8824(9) Å) are almost 0.1 Å longer than that of **5**. In both **3** and **5**, these values are longer than the sum of the covalent radii for a U–S single bond (2.73 Å),[76] and also longer than those in [$U^{III}(SMes^*)_3$] (2.7127(11) to 2.7247(10) Å) and complex **A** (2.7082(7) Å).[14,15] Lastly, the U–S distances in **5** are shorter than those in [$La(SAr^{iPr6})_2(I)$] (2.8235(12) and 2.8173(10) Å) by more than the difference in the ionic radii of U(III) (1.025 Å) and La(III) (1.032 Å), which is often ascribed to covalent contributions to the bonding in uranium complexes which are absent in the lanthanum congeners..[41,104] The U···B distance in **5** (2.872(4) Å) is larger than the other U(III) and U(IV) complexes presented herein, though it is similar to other terminal and bridging U–{κ^2-BH_4} distances previously reported for U(III) complexes.[54,55,57]

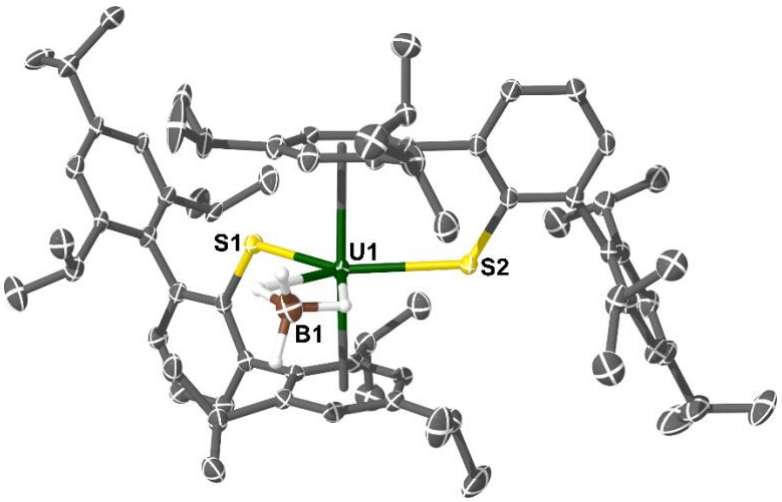

Figure 6. Molecular structure of complex **5**. Ellipsoids set at 50% probability and non-BH_4 H-atoms removed for clarity. Selected bond lengths and angles: U1–S1 = 2.7888(8) Å, U1–S2 = 2.7969(7) Å, U1···B1 = 2.872(4) Å, U1···$Tripp_{centroid1}$ = 2.744(2) Å, U1···$Tripp_{centroid2}$ = 2.747(2) Å, U1···S_2B-plane = 0.004(2) Å, S1–U1–S2 = 128.23(2)°, U1–S1–C_{ipso} = 118.15(11)°, U1–S2–C_{ipso} = 118.53(11)°, $Tripp_{centroid1}$···U1···$Tripp_{centroid2}$ = 176.79(4)°.

Table 1. Bond lengths (Å) and angles (°) for complexes **1**, **1·Et₂O**, **2**, **3**, **4a**, **4b**, and **5**.

(Å or °)	1 [A]	1·Et₂O	2	3	4a	4b [B]	5
U–S	2.675(5)	2.6526(9)	2.6948(10)	2.8824(9)	2.687(4)	2.721(3)	2.7888(8), 2.7969(7)
U···B	–	–	2.489(6) – 2.865(7)	2.584(6), 2.603(7)	2.56(2), 2.56(3)	2.556(8), 2.609(6)	2.872(4)
U–TrippC₆	– [C]	–	–	2.883(4) – 2.920(4)	2.815(16) – 2.918(17)	2.867(5) – 2.899(5)	3.030(3) – 3.152(3)
U···η⁶-Tripp$_{cent}$	2.591	–	–	2.5379	2.482	2.5168	2.744, 2.747
U–S–C$_{ipso}$	115.3(5), 123.3(6)	158.71(14)	124.88(14)	109.54(12)	113.6(5)	111.7(4)	118.53(11)

[A] Mean value of all ten independent molecules, and the ESD is given as the standard deviation of all the values. [B] The {SAr^{iPr6}} unit is disorder over two positions which refined to a ratio of 82:18, only metrics for the highest occupancy unit are given. [C] Not given due to the poor data quality.

UV-Vis-NIR spectroscopy

The UV-Vis-NIR spectra of complexes **1**, and **2-5** were recorded at room temperature as Et_2O solutions and are shown in **Figure 7**. Note that in the case of **2**, while exposure of the crude reaction mixture to Et_2O caused decomposition to $(SAr^{iPr6})_2$, this was not the case for isolated crystalline material.

The electronic absorption spectra for **1** and **2** are typical for U(IV): **1** features two broad charge transfer features with maxima at *ca.* 26,000 cm^{-1} (385 nm, ε *ca*. 1,800 M^{-1} cm^{-1}) and 20,000 cm^{-1} (500 nm, ε *ca*. 880 M^{-1} cm^{-1}) which tail off below 14,000 cm^{-1} (715 nm); and **2** displays a broad absorbance across the whole visible range which then tails off below 14,000 cm^{-1}. The NIR region for both feature weak Laporte-forbidden intra-configurational *f–f* transitions (**1**, ε *ca*. 15 M^{-1} cm^{-1}; **2**, ε *ca*. 100 M^{-1} cm^{-1}).[115-118] The UV-Vis region of complexes **3**, **4a**, and **4b** are remarkably similar, showing multiple strong overlapping absorptions with maxima centered around 22,880 cm^{-1} (437 nm), 21,000 cm^{-1} (476 nm), 19,940 cm^{-1} (502 nm), 18,115 cm^{-1} (552 nm), and *ca.* 16,195 cm^{-1} (617 nm) with molar absorptivity values (ε) ranging from *ca*. 400 to 1200 M^{-1} cm^{-1}. These broad features then tailing into the NIR region below 14,000 cm^{-1} (715 nm). The UV-Vis-NIR spectrum of **5** is similar to that of $[U(NHAr^{iPr6})_2(I)]$,[35] with a broad charge transfer feature at *ca.* 20,512 cm^{-1} (488 nm, ε *ca.* 1,333 M^{-1} cm^{-1}). The NIR region of the mono arylthiolate U(III) complexes **3**, **4a**, and **4b** features a broad series of poorly defined Laporte-forbidden intra-configurational *f–f* transitions (ε *ca*. 60 M^{-1} cm^{-1}). On the other hand, complex **5** shows well-defined features between 7,830 cm^{-1} (1,277 nm) and 12,173 cm^{-1} (821 nm; ε *ca.* 55–118 M^{-1} cm^{-1}).

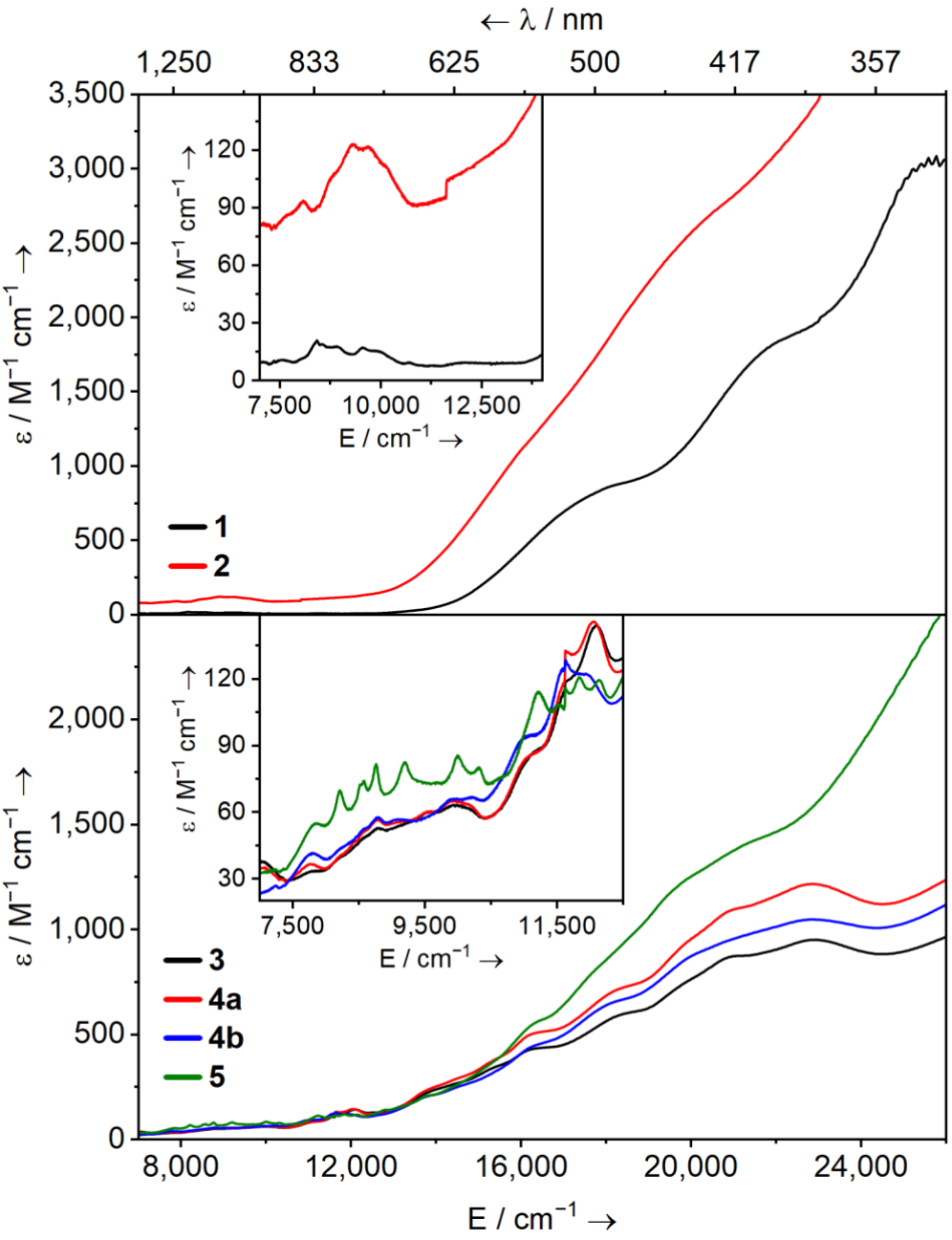

Figure 7. Solution UV-Vis-NIR spectra of U(IV) **1** and **2** (top panel), and **3**-**5** (bottom panel) – all as 1.0 mM (of U content) in Et_2O at ambient temperature.

SQUID magnetometry

We examined the magnetic properties of complexes **1**–**3**, **4b** and **5** using variable-temperature SQUID magnetometry (see **Figure 8**, and *Supporting Information*) to better

understand their ground state electronic structures as room temperature magnetic moments do not allow for the unambiguous assignment oxidation state in U(III) or U(IV) complexes.[119]

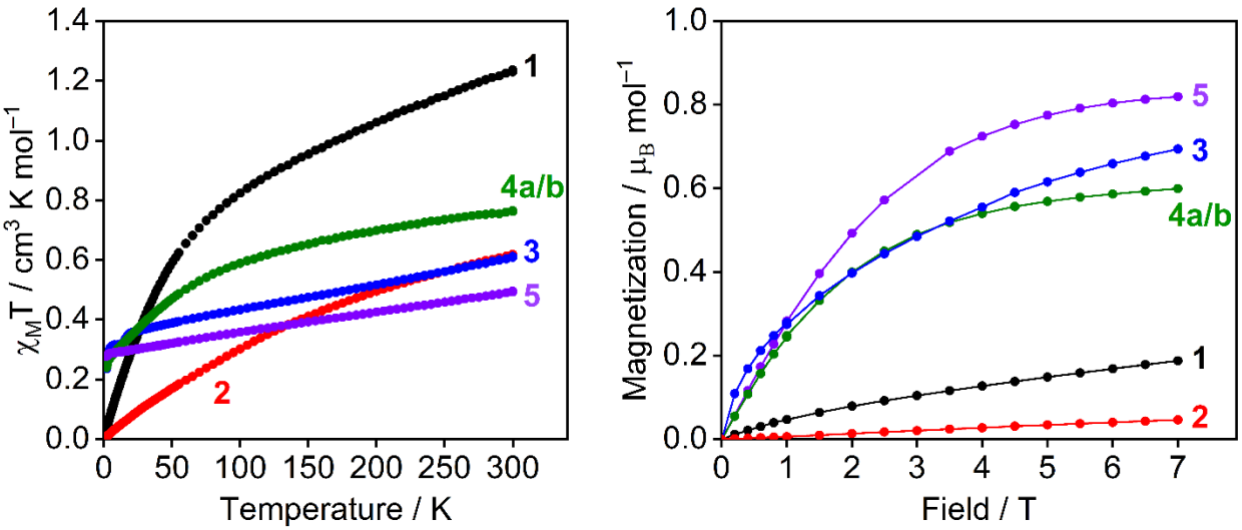

Figure 8. Variable temperature SQUID magnetic moment data (χT, left) over the temperature range 1.8–300 K in an applied field of 1000 Oe and magnetization (right) over the field range 0–7,000 Oe at 1.8 K for **1** (black), **2** (red), **3** (blue), **4a**/**b** (green), **5** (purple).

For U(IV) ($5f^2$, $^3H_4$ at the *LS* limit) complexes **1** and **2**, effective magnetic moments of 3.14 μB (1.24 cm^3 mol^{-1} K; **1**) and 2.22 μB (0.62 cm^3 mol^{-1} K; **2** per U ion) were measured at 300 K. These values decrease smoothly over the temperature range reaching 0.51μB (0.03 cm^3 mol^{-1} K; **1**) and 0.24 μB (0.01 cm^3 mol^{-1} K; **2** per U ion) at 1.8 K and tend to zero. This behavior is typical of the thermal depopulation of crystal field states of the split $^3H_4$ ground multiplet into an orbital singlet ground state, which is common for U(IV).[6,119] An isolated f^2 ion has an integer spin so can be an orbital singlet at low temperature, subject to temperature independent paramagnetism (TIP), resulting in non-zero magnetic moments. However, the magnetic profiles for **1** and **2** exhibit notable differences. The curve does not fall as quickly for **1** as it does for **2**, which is characteristic of strongly donating or charge-rich ligands exerting larger crystal field effects on U(IV) ions.[120] The effective magnetic

moments at 300 K for **1** and **2** differ significantly (3.14 μB vs. 2.22 μB both per U ion), and both are markedly reduced from the free-ion value (3.58 μB) which we attribute to crystal field effects resulting in different degrees of excited state mixing into the ground state.[121,122] Isothermal magnetization *vs* field measurements at 1.8 K for **1** and **2** exhibit low values of magnetization, with no sign of approaching saturation up to the highest field (0.19 μB mol^{-1} for **1** and 0.05 μB mol^{-1} per U ion for **2** at 7 T and 1.8 K) consistent with their non-Kramers U(IV) formulations. In short, all the data for **2** (see *Supporting Information*) suggests it contains two non-interacting U(IV) ions.

For U(III) ($5f^3$, $^4I_{9/2}$ at the *LS* limit) complexes **3** and **5**, effective magnetic moments of 1.99 μB (0.50 cm^3 mol^{-1} K; **3**) and 2.47 μB (0.76 cm^3 mol^{-1} K; **5**) were measured at 300 K. These values exhibit a slow reduction across the temperature range reaching 1.49 μB (0.28 cm^3 mol^{-1} K; **3**) and 1.39 μB (0.24 cm^3 mol^{-1} K; **5**) at 1.8 K. This is a result of the thermal depopulation of crystal field states of the $^4I_{9/2}$ ground multiplet into an orbital doublet ground state giving rise to higher (non-zero) low temperature moments, which is typical for U(III).[119,123] For both, the effective magnetic moment at 300 K is low compared to that of the theoretical U(III) $^4I_{9/2}$ free-ion value (3.62 μB); however, this has been observed for other arene-anchored U(III) complexes.[15,124,125] Isothermal magnetization *vs* field measurements for at 1.8 K **3** and **5** exhibit magnetization values commensurate with U(III) Kramers ion configurations, approaching saturation up to the highest field (0.82 μB mol^{-1} for **3** and 0.59 μB mol^{-1} for **5** at 7 T and 1.8 K).

In the case of **4a** and **4b**, ATR-IR data suggests that both are present in both batches of crystalline material. Given the difference between these two complexes is just one unit of H_2, their per-uranium magnetic properties should be comparable absent any exchange interactions through the $\{B_2H_6\}^{2-}$ bridge and so we have collected data for the **4a**/**b** mixture.

Both the low- and high-temperature magnetic susceptibility for **4a**/**b** (300 K: 2.21 μB, 0.61 cm^3 mol^{-1} K; and 1.8 K: 1.38 μB, 0.24 cm^3 mol^{-1} K – all per U ion) are in good agreement with those of **3** and **5**, and therefore for a U(III) composition. Likewise, the isothermal magnetization for **4a**/**b** approaches saturation at the highest fields, reaching 0.69 μB mol^{-1} per U ion at 7T and 1.8 K. The similarity of the per-ion magnetic profile to that of **3** and **5** suggests that if any magnetic communication between the two U-atoms is present, it is very weak, and that the magnetic contribution from **4b** to the data is what would be expected from a pair of magnetically isolated U(III) ions.

Electronic structure calculations

To better understand the nature of the U–S bonding and U···arene interaction in these complexes unrestricted Kohn-Sham density-functional theory (DFT) calculations were performed in ORCA 5.0[126] using the PBE0 functional[127,128] on H-atom optimized coordinates for **1·Et₂O** (*S* = 1), **2** (*S* = 2), **3**, **4a**, **5** (*S* = $^3/_2$), **4b** (*S* = 3) derived from the SC-XRD data. In the case of **1**, all coordinates were optimized due to the presence of ten crystallographically independent molecules (see *Supporting Information*). For complex **1**, the (mean) SC-XRD and calculated U–S and U–Cl distances differ by ≤0.005 Å except for the U–S linkage for the {SAr$^{i\text{Pr}}$} ligand with a U···η^6-Tripp contact which differs by 0.014 Å, though this is within 2σ of the mean and so represents a sound model.

Computational analyses of atomic charges derived from Kohn-Sham molecular orbitals (KS MOs) are fraught with difficulty,[129-132] and the differing coordination numbers in **1**–**5** preclude meaningful direct comparisons. However, a comparison of the Mulliken charges (Q_{AM}) and spin populations for the S-atoms (S_M S) is instructive towards the nature of their interaction with the U-atoms. In a similar fashion, the U-atom spin populations (S_M U) report whether

there is net exchange of spin density away from, or towards the metal. These data are summarized in **Table 2** along with the Mayer bond orders and the U–S bond lengths from SC-XRD, or calculation in the case of **1**. The U–S MBO values are broadly in agreement with other examples of U(III) and U(IV) thiolate linkages.[15,133]

Table 2. Spin population (S_M) and Mulliken atomic charge (Q_{AM}) analyses, and the U–S Mayer bond orders (MBO) and crystallographic bond lengths for the U–S linkages of complexes **1**-**5**.

Complex	S_M U	Q_{AM} S	S_M S	U–S MBO	U–S bond (Å)
1	2.23	–0.33 –0.45	–0.07 –0.08	1.04 0.86	2.678 [A] 2.653 [A]
1·Et₂O	2.23	–0.46 –0.46	–0.05 –0.05	0.76 0.76	2.6526(9)
2 [B]	2.20	–0.51	–0.06	0.82	2.6948(10)
3	3.06	–0.17	–0.02	0.50	2.8824(9)
4a	3.06	–0.39	–0.05	0.94	2.687(4)
4b [B]	3.04	–0.41	–0.04	0.97	2.721(3)
5	3.15	–0.41 –0.41	–0.04 –0.04	0.71 0.71	2.7888(8) 2.7969(7)

[A] Bond lengths from the fully optimized structure and so no ESD is given. [B] Values are given for only one of the U-atoms as there are no significant differences in these dimers.

The U-atom spin populations of 2.23, 2.23, and 2.20 for complexes **1**, **1·Et₂O**, and **2** respectively show they are net importers of spin density as all somewhat exceed the expected values of 2 for U(IV) $5f^2$, whereas values of 3.06, 3.06, and 3.04 for **3**, **4a**, and **4b** respectively are in good agreement with their U(III) $5f^3$ configurations. Complex **5** (3.15) is an outlier. These data show that: (i) there is a weak positive correlation between the number of S (and Cl) donors, and increased U-atom spin population; (ii) there is no clear correlation between the MBO and the U-atom oxidation state; (iii) complex **3**, for which the coordination

of BH_3 to the S-atom withdraws charge, and also complex **5**, possess the lowest U–S MBO values; (iv) complex **5** is the only U(III) complex with a notable deviation of the spin population from the ideal value.

While U···arene δ-bonding interactions are a common feature in low oxidation state uranium complexes with arene ligands,[6,15,33-35,38,40,125,134-141] inspection of the KS-MOs in all complexes herein reveals no δ or π U-arene overlap in the occupied orbitals, though most show such an interaction in their first unoccupied orbitals. This is likely due to the arene groups sitting further from the U(III) center (*e.g.* in **5**, U···$Tripp_{centroid}$ = 2.744 and 2.747 Å) than in similar complexes such as **A** (U···$Mes_{centroid}$ = 2.464 Å), or a recently reported U(III) *tris*-boryloxide complex (U···$arene_{centroid}$ = 2.616 Å) – both of which,[15,125] exhibit δ-bonding interactions.

Due to the delocalized nature of KS MOs we next turn to analysis of the U–S interactions using the natural bond order (NBO) and quantum theory of atoms in molecules (QTAIM) formalisms. Error! Reference source not found. reports the natural localized molecular orbitals (NLMOs) for the U–S σ- and π-components in complexes **1**–**5**. Note that such notation is a guide for the interaction symmetry and that the U–S overlap is often poorly oriented as has been observed elsewhere due to the low symmetry.[142,143] For complex **1**, the two inequivalent U–S bonds decompose into four NLMOs with U-contributions ranging from 14–20%, divided almost equally between 6*d* and 5*f* contributions in three of the four cases (the last being >60% U 5*f* – see **Figure 9**. In **1·Et₂O** the U–S π-bonding is prominent (**Figure 9**) with a U-content of 13.3% (38.28% 5*f*, 61.48% 6*d*) which is dominated by the 6*d* contribution. The corresponding σ-bond is poorly localised (U, 15.6%; 64.02% 5*f*, 31.31% 6*d*) and a larger 5*f* composition than in the π-bond.

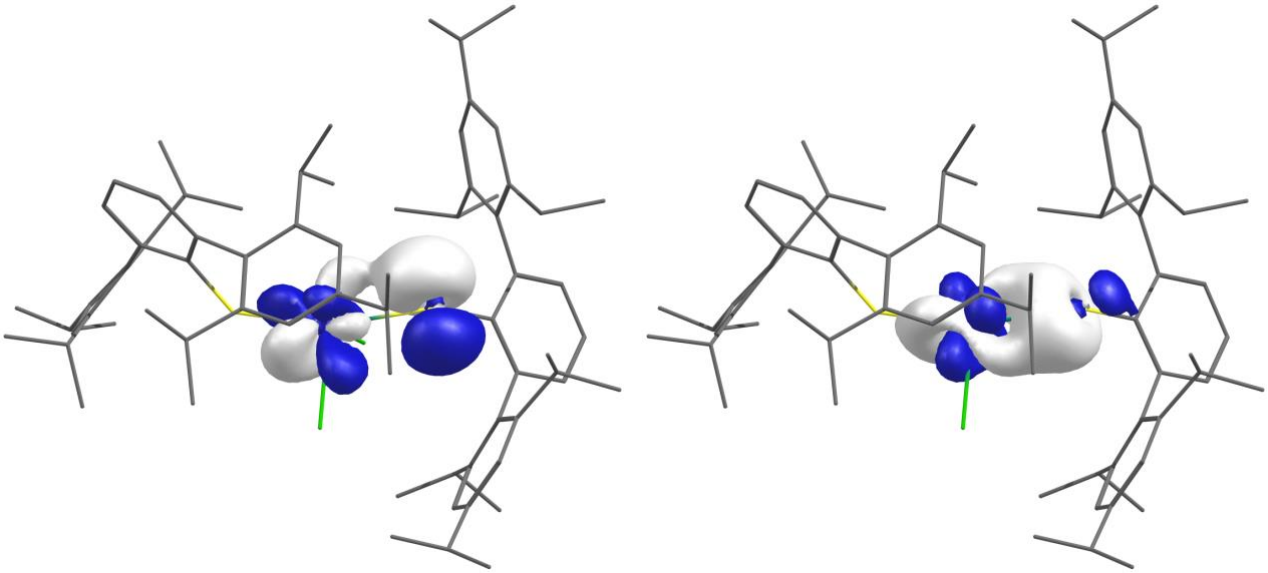

1 U1–S2 (NLMO150)

U (16.711%; 42.35% 5*f*, 57.13% 6*d*)

S (80.387%)

1 U1–S2 (NLMO151)

U (19.932%; 38.96% 5*f*, 44.78% 6*d*)

S (77.049%)

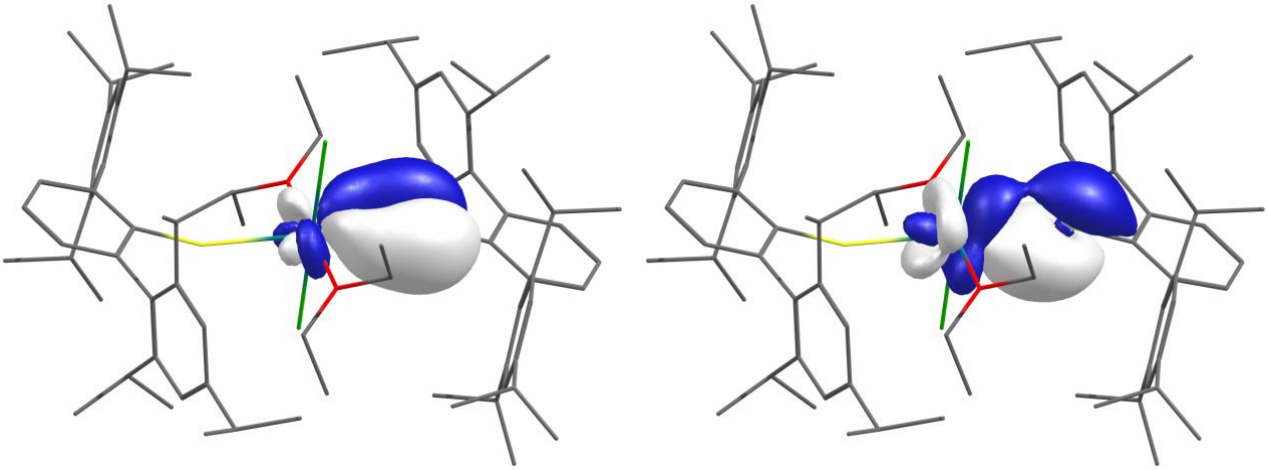

1·Et₂O U1–S1 (NLMO149)

U (13.277%; 38.28% 5*f*, 61.48% 6*d*)

S (84.055%)

1·Et₂O U1–S1 (NLMO150)

U (15.590%; 64.02% 5*f*, 31.31% 6*d*)

S (79.322%)

Figure 9. Selected NLMO isosurfaces (0.05 a.u.) for **1** (top) and **1·Et₂O** (bottom).

For complex **2** both σ- and π-components for the U–S bond were found, with the σ-bond (U, 25.431%; 34.53% 5*f*, 57.02% 6*d*) bearing a larger uranium (and 6*d*) component than the corresponding π-bond (U, 14.193%; 61.94% 5*f*, 37.51% 6*d*). In complex **3**, the BH_3 group

occupies the S-atom lone pair and only a U–S σ-bond is found (U, 16.155%; 28.64% 5*f*, 63.81% 6*d*). Despite this lone pair being available for U–S π-bonding in the case of complex **4a**, we find two poorly oriented interactions (12.022% and 18.378% U-character) with approximate σ-symmetry which compare well to the U–S σ-bond in **3** – all show dominant U 6*d* character as would be expected from Bursten's FEUDAL description of actinide bonding (see **Figure 10** for both **3** and **4a**).[144] Complex **4b** is comparable to **4a**, and so the data are presented in the *Supporting Information*. Finally, in complex **5** we find each U–S interaction is spread across three NLMOs, each showing poor orientation of the respective parent atomic orbitals and low U-content (3.708–10.492%). At low isovalues (<0.03 a.u.) U–S π-bonds can be seen, but clearly the interaction is essentially ionic in nature due to the poor overlap. NLMO compositions are collated in **Table S16**.

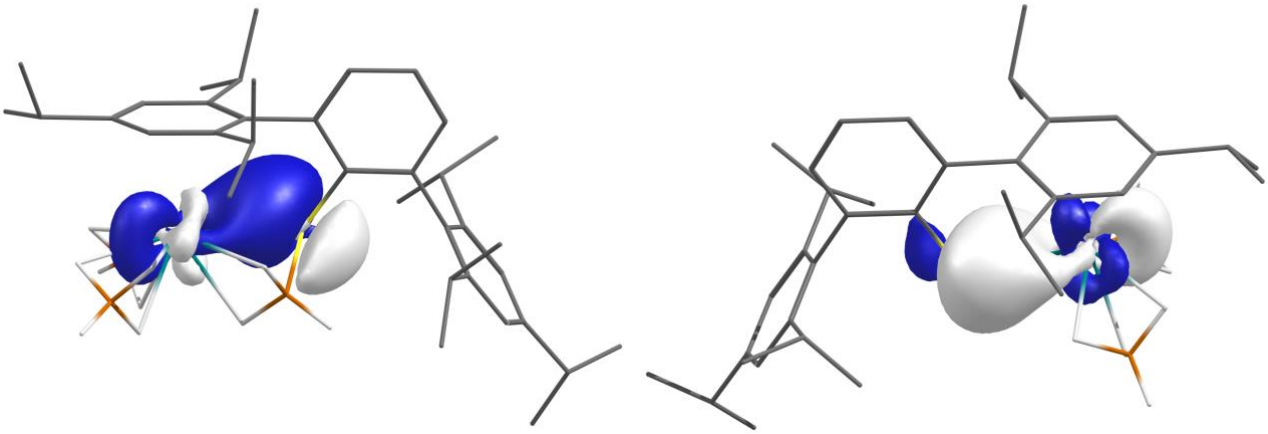

3 U1–S1 (NLMO92)

U (16.155%; 28.64% 5*f*, 63.81% 6*d*)

S (79.781%)

4a U1–S1 (NLMO92)

U (18.378%; 21.02% 5*f*, 65.86% 6*d*)

S (78.885%)

Figure S10. Selected NLMO isosurfaces (0.05 a.u.) for **3** (left) and **4a** (right).

Bader's Quantum Theory of Atoms In Molecules (QTAIM), is a topological analysis of the surface density between atoms and provides intuitive definitions and metrics for chemical bonding. A combination of these metrics can paint a picture of the nature of the chemical

bond, and is a complementary technique to the NBO and NLMO analysis above. Here, we focus on the delocalization index (δ), electron density (ρ), energy density (H), and the QTAIM charges for the U- and S-atoms of each complex.[132] The δ(U,S) for the U–S bonds in **1** (0.761, 0.807) are larger than for **1·Et₂O** (0.690), and this is reflected at the bond critical points (BCPs) where for **1** both ρ (0.072, 0.072) and H (–0.019, –0.019) are larger in magnitude than in **1·Et₂O** (ρ = 0.060, H = –0.012). For both U(IV) complexes, the U–S interactions are polar as indicated by the small ρ values and positive values for the Laplacian of the electron density ($\nabla^2\rho$); however, the modest values for δ(U,S), and negative H-values describe some covalent contributions. For complex **2**, δ(U,S) (0.699), ρ (0.067), and H (–0.016) lie between those of **1** and **1·Et₂O**. These metrics and others are summarized in **Table 3**.

Table 3. QTAIM charges, electron densities (ρ), energy densities (H), ellipticity, and delocalization (δ) and localization indices of complexes **1**–**5**.

Complex	QTAIM charge (U/S)	ρ	$\nabla^2\rho$	H	δ(U,S)	LI(U)
1	+2.160/–0.438 +2.160/–0.541	0.072 0.073	0.0914 0.099	–0.019	0.761 0.804	87.717
1·Et₂O	+2.354/–0.567	0.060	0.137	–0.012	0.690 0.691	87.622
2	+2.271/–0.556	0.067	0.096	–0.016	0.699 0.700	87.603
3	+1.968/–0.535	0.044	0.095	–0.007	0.397	88.197
4a	+1.960/–0.498	0.065	0.110	–0.016	0.671	88.295
4b	+1.944/–0.498 +1.943/–0.498	0.063 0.063	0.104 0.104	–0.015 –0.015	0.634 0.635	88.232
5	+1.935/–0.533	0.055 0.054	0.101 0.099	–0.011	0.570 0.563	88.475

When comparing the U(IV) complexes above, to U(III) complexes **3**, **4a**, **4b**, and **5**, we observe a decrease in all topological metrics measured. The effect of the S-bound BH_3 group in **3** is pronounced as ρ (0.044), H (–0.007), and δ(U,S) (0.397) are significantly reduced compared to those in **4a** (0.065, –0.016, 0.671 respectively), though QTAIM metrics are highly M–X distance dependent and the U–S length in **3** is longer than the others. There are negligible differences in the U–S bonds between complexes **4a** and **4b** (see **Table 3**). Analysis of complex **5** reveals U–S bonding somewhat more ionic than the other complexes herein, though again the U–S distance is somewhat longer than for other complexes. Metrics for the U–S bonding in the U(III) complexes here are similar to those reported elsewhere.[15,133]

The localization index, LI, can be used to examine the metal–element linkages. Deviations in the value returned for the metal indicate charge transfer interactions. For a pure ionic system, values of 88 and 89 for U(IV) and U(III) respectively would be expected. Reduced values are found for all complexes, with deviations of 0.28–0.40 for the U(IV) complexes (**1**, **1·Et₂O**, and **2**) and 0.52–0.80 for the U(III) systems (**3**, **4a**, **4b**, and **5**), suggesting charge transfer, and is in line with qualifying covalent assessments made earlier. Meyer and co-workers have used this metric to assess the U(III) arene-anchored *tris*-thiophenolate complex, $[U^{III}\{(SAr^{Ad,Me})_3Mes\}]$, with a reported LI(U) of 88.25 (a deviation of 0.75).[15]

Conclusions

In summary, we have expanded the field of molecular uranium organo-sulfur complexes, demonstrating diverse bonding modes and coordination environments facilitated by the weakly coordinating arene rings of the $\{SAr^{iPr6}\}$ *meta*-terphenyl framework including

examples of both the shortest and one of the longest U^{III}–S distances to date for anionic sulfur donors.

Limited success was found in using $U^{IV}Cl_4$ in salt elimination reactions with two equivalents of $KSAr^{iPr6}$ for the isolation of U(IV) complexes, with both $[U^{IV}(SAr^{iPr6})_2(Cl)_2]$ and $[U^{IV}(SAr^{iPr6})_2(Cl)_2(Et_2O)_2]$ being obtained in low yield. While the reaction between $[U^{IV}(BH_4)_4]$ and one equivalent of $KSAr^{iPr6}$ gave the double salt $[U^{IV}(\mu\text{-}SAr^{iPr6})(BH_4)_2(\mu\text{-}BH_4)(\mu^3\text{-}BH_4)K]_2$ in toluene, or oxidative coupling to give $(SAr^{iPr6})_2$ in Et_2O, one equivalent of $HSAr^{iPr6}$ reacted with $[U^{IV}(BH_4)_4]$ under thermal conditions in toluene to give the U(III) sulfur-borane complex $[U^{III}(H_3B{\cdot}SAr^{iPr6}\text{-}\kappa S,H,H)(BH_4)_2]$, the first such example with an *f*-element complex. Salt elimination using $[U^{III}(BH_4)_3(toluene)]$ and one equivalent of $KSAr^{iPr6}$ allowed access to borane-free $[U^{III}(SAr^{iPr6})(BH_4)_2]$ which appears to undergo slow thermolysis to $[\{U^{III}(SAr^{iPr6})(BH_4)\}_2(\mu\text{-}B_2H_6)]$. The latter complex contains a diborane(6) dianion and is the first example of an *f*-element *nido*-metalloborane. The *bis*-arylthiolate complex $[U^{III}(SAr^{iPr6})_2(BH_4)]$ bearing two U···arene interactions was isolated from the reaction between $[U^{III}(BH_4)_3(toluene)]$ and two equivalents of $KSAr^{iPr6}$.

Quantum chemical analysis of the U–S bonding in all complexes reveals polar covalent interactions with both σ- and π-contributions to the bonding in some cases, though low symmetry in all complexes precludes efficient orbital overlap. In $[U^{III}(H_3B{\cdot}SAr^{iPr6}\text{-}\kappa S,H,H)(BH_4)_2]$, the Lewis-acid capping of the S-donor significantly reduces bonding to the U-atom. Despite the prevalence of U-arene interactions in the molecular structures of most complexes herein, no substantial U-arene π- or δ-bonding interactions were found within the occupied molecular orbitals, and a topological analysis corroborated this.

Conflicts of Interest

There are no conflicts to declare.

Acknowledgements

We thank the Royal Society for funding PostDoctoral funding (B.L.L.R.) and a University Research Fellowship (URF\211271 to C.A.P.G.). We acknowledge funding from the EPSRC (EP/K039547/1, EP/V007580/1, EP/P001386/1, and EP/K039547/1 for NMR spectroscopy and X-ray diffraction). We also thank the EPSRC UK EPR National Research Facility for access and use of the SQUID magnetometer (EP/W014521/1, EP/V035231/1, EPS033181/1). C.A.P.G. thanks the Computational Shared Facility at the University of Manchester for support. We thank Prof. Stephen Liddle for support (J.A.S.), and Prof. Nik Kaltsoyannis for advice. Elemental analyses were performed at the UoM by Mr Martin Jennings and Ms Anne Davies.

Supporting Information

See the *Supporting Information* for details of the starting materials used, synthesis of complexes described, descriptions of sample preparation for spectroscopic measurements, and methodologies for the DFT calculations. The following CCDC references contain the supplementary crystal data for this article: **1** (2352695), **1·Et$_2$O** (2352696), **2** (2352697), **3** (2352698), **4a** (2352699), **4b** (2352700), **5** (2352701), [U^{IV}(BH$_4$)$_2${μ-B$_2$H$_6$}]$_n$ (2352702), and (SAr^{iPr6})$_2$ (2352703). These data can be obtained free of charge from the Cambridge Crystallographic Data Centre via *www.ccdc.cam.ac.uk/data_request/cif*. Raw experimental data (NMR, ATR-IR, UV-Vis-NIR, SQUID Magnetometry) and computational inputs/outputs can be found freely at DOI:10.48420/26321476.

References

(1) Goodwin, C. A. P.; Mills, D. P. Silylamides: towards a half-century of stabilising remarkable f-element chemistry. In *Specialist Periodical Reports: Organometallic Chemistry*, Organometallic Chemistry, Vol. 41; Royal Society of Chemistry, 2017; pp 123-156.

(2) Liddle, S. T.; Mills, D. P.; Natrajan, L. S. *The Lanthanides and Actinides*; World Scientific Publishing Europe Ltd., 2022. DOI: https://doi.org/10.1142/q0298.

(3) Bradley, D. C.; Mehrotra, R. C.; Rothwell, I. P.; Singh, A. *Alkoxo and Aryloxo Derivatives of Metals*; 2001. DOI: https://doi.org/10.1016/B978-0-12-124140-7.X5000-2.

(4) Löffler, S. T.; Meyer, K. 3.13 - Actinides. In *Comprehensive Coordination Chemistry III*, Constable, E. C., Parkin, G., Que Jr, L. Eds.; Elsevier, 2021; pp 471-521.

(5) Berthet, J. C.; Ephritikhine, M. New advances in the chemistry of uranium amide compounds. *Coord. Chem. Rev.* **1998**, *178-180*, 83-116. DOI: https://doi.org/10.1016/S0010-8545(98)00061-7

(6) Liddle, S. T. The Renaissance of Non-Aqueous Uranium Chemistry. *Angew. Chem., Int. Ed.* **2015**, *54*, 8604-8641. DOI: https://doi.org/10.1002/anie.201412168

(7) Mathur, J. N.; Murali, M. S.; Nash, K. L. Actinide Partitioning—a Review. *Solvent Extr. Ion Exch.* **2007**, *19*, 357-390. DOI: https://doi.org/10.1081/SEI-100103276

(8) Nilsson, M.; Nash, K. L. Review Article: A Review of the Development and Operational Characteristics of the TALSPEAK Process. *Solvent Extr. Ion Exch.* **2007**, *25*, 665-701. DOI: https://doi.org/10.1080/07366290701634636

(9) Philip Horwitz, E.; Kalina, D. C.; Diamond, H.; Vandegrift, G. F.; Schulz, W. W. The TRUEX process - A process for the extraction of the transuranic elements from nitric acid wastes utilizing modified PUREX solvent. *Solvent Extr. Ion Exch.* **2007**, *3*, 75-109. DOI: https://doi.org/10.1080/07366298508918504

(10) Chen, J.; Wang, S.; Xu, C.; Wang, X.; Feng, X. Separation of Americium from Lanthanides by Purified Cyanex 301 Countercurrent Extraction in Miniature Centrifugal Contactors. *Procedia Chemistry* **2012**, *7*, 172-177. DOI: https://doi.org/10.1016/j.proche.2012.10.029

(11) Bhattacharyya, A.; Mohapatra, P. K. Separation of trivalent actinides and lanthanides using various 'N', 'S' and mixed 'N,O' donor ligands: a review. *Radiochim. Acta* **2019**, *107*, 931-949. DOI: https://doi.org/10.1515/ract-2018-3064

(12) Dam, H. H.; Reinhoudt, D. N.; Verboom, W. Multicoordinate ligands for actinide/lanthanide separations. *Chem. Soc. Rev.* **2007**, *36*, 367-377. DOI: https://doi.org/10.1039/B603847F

(13) Gaunt, A. J.; Scott, B. L.; Neu, M. P. Homoleptic uranium(III) imidodiphosphinochalcogenides including the first structurally characterised molecular trivalent actinide-Se bond. *Chem. Commun.* **2005**, 3215-3217. DOI: https://doi.org/10.1039/B503106K

(14) Roger, M.; Barros, N.; Arliguie, T.; Thuery, P.; Maron, L.; Ephritikhine, M. U(SMes*)$_n$, (n = 3, 4) and Ln(SMes*)$_3$ (Ln = La, Ce, Pr, Nd): lanthanide(III)/actinide(III) differentiation in agostic interactions and an unprecedented η^3 ligation mode of the arylthiolate ligand, from X-ray diffraction and DFT analysis. *J. Am. Chem. Soc.* **2006**, *128*, 8790-8802. DOI: https://doi.org/10.1021/ja0584830

(15) Pividori, D.; Miehlich, M. E.; Kestel, B.; Heinemann, F. W.; Scheurer, A.; Patzschke, M.; Meyer, K. Uranium Going the Soft Way: Low-Valent Uranium(III) Coordinated to an Arene-Anchored Tris-Thiophenolate Ligand. *Inorg. Chem.* **2021**, *60*, 16455-16465. DOI: https://doi.org/10.1021/acs.inorgchem.1c02310

(16) Arliguie, T.; Fourmigué, M.; Ephritikhine, M. The First Dithiolene Complexes of an f-Element, Including the Cyclooctatetraene Derivative [Na(18-crown-6)(THF)][U(η^8-

$C_8H_8)(C_4H_4S_4)_2$], a Unique Example of a Uranium(V) Compound with Metal−Sulfur Bonds. *Organometallics* **2000**, *19*, 109-111. DOI: https://doi.org/10.1021/om990719j

(17) Boreen, M. A.; Parker, B. F.; Hohloch, S.; Skeel, B. A.; Arnold, J. f-Block complexes of a m-terphenyl dithiocarboxylate ligand. *Dalton Trans.* **2018**, *47*, 96-104. DOI: https://doi.org/10.1039/C7DT04073C

(18) Lescop, C.; Arliguie, T.; Lance, M.; Nierlich, M.; Ephritikhine, M. Bispentamethylcyclopentadienyl uranium(IV) thiolate compounds. Synthesis and reactions with CO_2 and CS_2. *J. Organomet. Chem.* **1999**, *580*, 137-144. DOI: https://doi.org/10.1016/S0022-328X(98)01139-5

(19) Matson, E. M.; Fanwick, P. E.; Bart, S. C. Formation of Trivalent U–C, U–N, and U–S Bonds and Their Reactivity toward Carbon Dioxide and Acetone. *Organometallics* **2011**, *30*, 5753-5762. DOI: https://doi.org/10.1021/om200612h

(20) Kiernicki, J. J.; Harwood, J. S.; Fanwick, P. E.; Bart, S. C. Reductive silylation of Cp*UO_2(MesPDIMe) promoted by Lewis bases. *Dalton Trans.* **2016**, *45*, 3111-3119. DOI: https://doi.org/10.1039/C5DT04776E

(21) Wang, D.; Wang, S.; Hou, G.; Zi, G.; Walter, M. D. A Lewis Base Supported Terminal Uranium Phosphinidene Metallocene. *Inorg. Chem.* **2020**, *59*, 14549-14563. DOI: https://doi.org/10.1021/acs.inorgchem.0c02363

(22) Rosenzweig, M. W.; Scheurer, A.; Lamsfus, C. A.; Heinemann, F. W.; Maron, L.; Andrez, J.; Mazzanti, M.; Meyer, K. Uranium(IV) terminal hydrosulfido and sulfido complexes: insights into the nature of the uranium–sulfur bond. *Chem. Sci.* **2016**, *7*, 5857-5866. DOI: https://doi.org/10.1039/C6SC00677A

(23) Rosenzweig, M. W.; Hümmer, J.; Scheurer, A.; Lamsfus, C. A.; Heinemann, F. W.; Maron, L.; Mazzanti, M.; Meyer, K. A complete series of uranium(IV) complexes with terminal hydrochalcogenido (EH) and chalcogenido (E) ligands E = O, S, Se, Te. *Dalton Trans.* **2019**, *48*, 10853-10864. DOI: https://doi.org/10.1039/C9DT00530G

(24) Diaconescu, P. L.; Arnold, P. L.; Baker, T. A.; Mindiola, D. J.; Cummins, C. C. Arene-Bridged Diuranium Complexes: Inverted Sandwiches Supported by δ Backbonding. *J. Am. Chem. Soc.* **2000**, *122*, 6108-6109. DOI: https://doi.org/10.1021/ja994484e

(25) Brown, J. L.; Fortier, S.; Wu, G.; Kaltsoyannis, N.; Hayton, T. W. Synthesis and spectroscopic and computational characterization of the chalcogenido-substituted analogues of the uranyl ion, $[OUE]^{2+}$ (E = S, Se). *J. Am. Chem. Soc.* **2013**, *135*, 5352-5355. DOI: https://doi.org/10.1021/ja402068j

(26) Smiles, D. E.; Wu, G.; Hayton, T. W. Synthesis of uranium-ligand multiple bonds by cleavage of a trityl protecting group. *J. Am. Chem. Soc.* **2014**, *136*, 96-99. DOI: https://doi.org/10.1021/ja411423a

(27) Smiles, D. E.; Wu, G.; Hayton, T. W. Synthesis of Terminal Monochalcogenide and Dichalcogenide Complexes of Uranium Using Polychalcogenides, $[En]^{2-}$ (E = Te, *n* = 2; E = Se, *n* = 4), as Chalcogen Atom Transfer Reagents. *Inorg. Chem.* **2014**, *53*, 10240-10247. DOI: https://doi.org/10.1021/ic501267f

(28) Gardner, B. M.; King, D. M.; Tuna, F.; Wooles, A. J.; Chilton, N. F.; Liddle, S. T. Assessing crystal field and magnetic interactions in diuranium-μ-chalcogenide triamidoamine complexes with U^{IV}–E–U^{IV} cores (E = S, Se, Te): implications for determining the presence or absence of actinide–actinide magnetic exchange. *Chem. Sci.* **2017**, *8*, 6207-6217. DOI: https://doi.org/10.1039/C7SC01998J

(29) Ephritikhine, M. Molecular actinide compounds with soft chalcogen ligands. *Coord. Chem. Rev.* **2016**, *319*, 35-62. DOI: https://doi.org/10.1016/j.ccr.2016.04.020

(30) MacDonald, M. R.; Fieser, M. E.; Bates, J. E.; Ziller, J. W.; Furche, F.; Evans, W. J. Identification of the +2 oxidation state for uranium in a crystalline molecular complex, [K(2.2.2-cryptand)][$(C_5H_4SiMe_3)_3U$]. *J. Am. Chem. Soc.* **2013**, *135*, 13310-13313. DOI: https://doi.org/10.1021/ja406791t

(31) Windorff, C. J.; MacDonald, M. R.; Meihaus, K. R.; Ziller, J. W.; Long, J. R.; Evans, W. J. Expanding the Chemistry of Molecular U^{2+} Complexes: Synthesis, Characterization, and Reactivity of the $\{[C_5H_3(SiMe_3)_2]_3U\}^-$ Anion. *Chem. Eur. J.* **2016**, *22*, 772-782. DOI: https://doi.org/10.1002/chem.201503583

(32) Guo, F. S.; Tsoureas, N.; Huang, G. Z.; Tong, M. L.; Mansikkamaki, A.; Layfield, R. A. Isolation of a Perfectly Linear Uranium(II) Metallocene. *Angew. Chem., Int. Ed.* **2020**, *59*, 2299-2303. DOI: https://doi.org/10.1002/anie.201912663

(33) La Pierre, H. S.; Scheurer, A.; Heinemann, F. W.; Hieringer, W.; Meyer, K. Synthesis and characterization of a uranium(II) monoarene complex supported by δ backbonding. *Angew. Chem., Int. Ed.* **2014**, *53*, 7158-71562. DOI: https://doi.org/10.1002/anie.201402050

(34) Straub, M. D.; Ouellette, E. T.; Boreen, M. A.; Britt, R. D.; Chakarawet, K.; Douair, I.; Gould, C. A.; Maron, L.; Del Rosal, I.; Villarreal, D.; Minasian, S. G.; Arnold, J. A Uranium(II) Arene Complex That Acts as a Uranium(I) Synthon. *J. Am. Chem. Soc.* **2021**, *143*, 19748-19760. DOI: https://doi.org/10.1021/jacs.1c07854

(35) Billow, B. S.; Livesay, B. N.; Mokhtarzadeh, C. C.; McCracken, J.; Shores, M. P.; Boncella, J. M.; Odom, A. L. Synthesis and Characterization of a Neutral U(II) Arene Sandwich Complex. *J. Am. Chem. Soc.* **2018**, *140*, 17369-17373. DOI: https://doi.org/10.1021/jacs.8b10888

(36) Wedal, J. C.; Moore, W. N. G.; Lukens, W. W.; Evans, W. J. Perplexing EPR Signals from $5f^36d^1$ U(II) Complexes. *Inorg. Chem.* **2024**. DOI: https://doi.org/10.1021/acs.inorgchem.3c03449

(37) Wedal, J. C.; Furche, F.; Evans, W. J. Density Functional Theory Analysis of the Importance of Coordination Geometry for $5f^36d^1$ versus $5f^4$ Electron Configurations in U(II) Complexes. *Inorg. Chem.* **2021**, *60*, 16316-16325. DOI: https://doi.org/10.1021/acs.inorgchem.1c02161

(38) Chowdhury, S. R.; Goodwin, C. A. P.; Vlaisavljevich, B. What is the nature of the uranium(III)–arene bond? *Chem. Sci.* **2024**, *15*, 1810-1819. DOI: https://doi.org/10.1039/D3SC04715F

(39) MacKenzie, R. E.; Hajdu, T.; Seed, J. A.; Whitehead, G. F. S.; Adams, R. W.; Chilton, N. F.; Collison, D.; McInnes, E. J. L.; Goodwin, C. A. P. δ-Bonding versus Electron Localization in Formally Divalent Rare Earth Complexes. **2024**, *ChemRxiv DOI: 10.26434/chemrxiv-2024-6twmx*. DOI: https://doi.org/10.26434/chemrxiv-2024-6twmx

(40) Keener, M.; Shivaraam, R. A. K.; Rajeshkumar, T.; Tricoire, M.; Scopelliti, R.; Zivkovic, I.; Chauvin, A. S.; Maron, L.; Mazzanti, M. Multielectron Redox Chemistry of Uranium by Accessing the +II Oxidation State and Enabling Reduction to a U(I) Synthon. *J. Am. Chem. Soc.* **2023**, *145*, 16271-16283. DOI: https://doi.org/10.1021/jacs.3c05626

(41) Gilbert-Bass, K.; Stennett, C. R.; Grotjahn, R.; Ziller, J. W.; Furche, F.; Evans, W. J. Exploring sulfur donor atom coordination chemistry with La(II), Nd(II), and Tm(II) using a terphenylthiolate ligand. *Chem. Commun.* **2024**. DOI: https://doi.org/10.1039/D4CC01037J

(42) Twamley, B.; Haubrich, S. T.; Power, P. P. Element Derivatives of Sterically Encumbering Terphenyl Ligands. In *Advances in Organometallic Chemistry Volume 44*, Advances in Organometallic Chemistry, 1999; pp 1-65.

(43) Barnett, B. R.; Mokhtarzadeh, C. C.; Lummis, P.; Wang, S.; Queen, J. D.; Gavenonis, J.; Schüwer, N.; Tilley, T. D.; Boynton, J. N.; Weidemann, N.; Agnew, D. W.; Smith, P. W.; Ditri, T. B.; Carpenter, A. E.; Pratt, J. K.; Mendelson, N. D.; Figueroa, J. S.; Power, P. P. TERPHENYL LIGANDS AND COMPLEXES. In *Inorganic Syntheses*, Inorganic Syntheses, 2018; pp 85-122.

(44) Jena, R.; Benner, F.; Delano, F.; Holmes, D.; McCracken, J.; Demir, S.; Odom, A. L. A rare isocyanide derived from an unprecedented neutral yttrium(II) bis(amide)

complex. *Chem. Sci.* **2023**, *14*, 4257-4264. DOI: https://doi.org/10.1039/D3SC00171G

(45) Cantat, T.; Scott, B. L.; Kiplinger, J. L. Convenient access to the anhydrous thorium tetrachloride complexes $ThCl_4(DME)_2$, $ThCl_4(1,4\text{-dioxane})_2$ and $ThCl_4(THF)_{3.5}$ using commercially available and inexpensive starting materials. *Chem. Commun.* **2010**, *46*, 919-921. DOI: https://doi.org/10.1039/B923558B

(46) Patel, D.; Wooles, A. J.; Hashem, E.; Omorodion, H.; Baker, R. J.; Liddle, S. T. Comments on reactions of oxide derivatives of uranium with hexachloropropene to give UCl_4. *New J. Chem.* **2015**, *39*, 7559-7562. DOI: https://doi.org/10.1039/C5NJ00476D

(47) Fetrow, T. V.; Grabow, J. P.; Leddy, J.; Daly, S. R. Convenient Syntheses of Trivalent Uranium Halide Starting Materials without Uranium Metal. *Inorg. Chem.* **2021**, *60*, 7593-7601. DOI: https://doi.org/10.1021/acs.inorgchem.1c00598

(48) Schnaars, D. D.; Wu, G.; Hayton, T. W. Reactivity of UH_3 with mild oxidants. *Dalton Trans.* **2008**, 6121-6126. DOI: https://doi.org/10.1039/B809184F

(49) Carmichael, C. D.; Jones, N. A.; Arnold, P. L. Low-valent uranium iodides: straightforward solution syntheses of UI_3 and UI_4 etherates. *Inorg. Chem.* **2008**, *47*, 8577-8579. DOI: https://doi.org/10.1021/ic801138e

(50) Ortu, F. Rare Earth Starting Materials and Methodologies for Synthetic Chemistry. *Chem. Rev.* **2022**, *122*, 6040-6116. DOI: https://doi.org/10.1021/om060262v

(51) Emerson-King, J.; Gransbury, G. K.; Whitehead, G. F. S.; Vitorica-Yrezabal, I. J.; Rouzières, M.; Clérac, R.; Chilton, N. F.; Mills, D. P. Isolation of a Bent Dysprosium Bis(amide) Single-Molecule Magnet. *J. Am. Chem. Soc.* **2024**. DOI: https://doi.org/10.1021/jacs.3c12427

(52) Goodwin, C. A. P.; Reta, D.; Ortu, F.; Liu, J.; Chilton, N. F.; Mills, D. P. Terbocenium: completing a heavy lanthanide metallocenium cation family with an alternative anion

abstraction strategy. *Chem. Commun.* **2018**, *54*, 9182-9185. DOI: https://doi.org/10.1039/c8cc05261a

(53) Arnold, P. L.; Stevens, C. J.; Bell, N. L.; Lord, R. M.; Goldberg, J. M.; Nichol, G. S.; Love, J. B. Multi-electron reduction of sulfur and carbon disulfide using binuclear uranium(III) borohydride complexes. *Chem. Sci.* **2017**, *8*, 3609-3617. DOI: https://doi.org/10.1039/C7SC00382J

(54) Arliguie, T.; Belkhiri, L.; Bouaoud, S.-E.; Thuéry, P.; Villiers, C.; Boucekkine, A.; Ephritikhine, M. Lanthanide(III) and Actinide(III) Complexes $[M(BH_4)_2(THF)_5][BPh_4]$ and $[M(BH_4)_2(18\text{-crown-6})][BPh_4]$ (M = Nd, Ce, U): Synthesis, Crystal Structure, and Density Functional Theory Investigation of the Covalent Contribution to Metal-Borohydride Bonding. *Inorg. Chem.* **2009**, *48*, 221-230. DOI: https://doi.org/10.1021/ic801685v

(55) Boronski, J. T.; Doyle, L. R.; Seed, J. A.; Wooles, A. J.; Liddle, S. T. f-Element Half-Sandwich Complexes: A Tetrasilylcyclobutadienyl–Uranium(IV)–Tris(tetrahydroborate) Anion Pianostool Complex. *Angew. Chem., Int. Ed.* **2020**, *59*, 295-299. DOI: https://doi.org/10.1002/anie.201913640

(56) Ephritikhine, M. Synthesis, Structure, and Reactions of Hydride, Borohydride, and Aluminohydride Compounds of the f-Elements. *Chem. Rev.* **1997**, *97*, 2193-2242. DOI: https://doi.org/10.1021/cr960366n

(57) Arnold, P. L.; Stevens, C. J.; Farnaby, J. H.; Gardiner, M. G.; Nichol, G. S.; Love, J. B. New chemistry from an old reagent: mono- and dinuclear macrocyclic uranium(III) complexes from $[U(BH_4)_3(THF)_2]$. *J. Am. Chem. Soc.* **2014**, *136*, 10218-10221. DOI: https://doi.org/10.1021/ja504835a

(58) Baudry, D.; Bulot, E.; Charpin, P.; Ephritikhine, M.; Lance, M.; Nierlich, M.; Vigner, J. Arene uranium borohydrides: synthesis and crystal structure of $(\eta\text{-}C_6Me_6)U(BH_4)_3$. *J.*

Organomet. Chem. **1989**, *371*, 155-162. DOI: https://doi.org/10.1016/0022-328X(89)88022-2

(59) Haaland, A.; Shorokhov, D. J.; Tutukin, A. V.; Volden, H. V.; Swang, O.; McGrady, G. S.; Kaltsoyannis, N.; Downs, A. J.; Tang, C. Y.; Turner, J. F. C. Molecular Structures of Two Metal Tetrakis(tetrahydroborates), $Zr(BH_4)_4$ and $U(BH_4)_4$: Equilibrium Conformations and Barriers to Internal Rotation of the Triply Bridging BH_4 Groups. *Inorg. Chem.* **2002**, *41*, 6646-6655. DOI: https://doi.org/10.1021/ic020357z

(60) Bernstein, E. R.; Hamilton, W. C.; Keiderling, T. A.; La Placa, S. J.; Lippard, S. J.; Mayerle, J. J. 14-Coordinate uranium(IV). Structure of uranium borohydride by single-crystal neutron diffraction. *Inorg. Chem.* **1972**, *11*, 3009-3016. DOI: https://doi.org/10.1021/ic50118a027

(61) Bernstein, E. R.; Keiderling, T. A.; Lippard, S. J.; Mayerle, J. J. Structure of uranium borohydride by single-crystal x-ray diffraction. *J. Am. Chem. Soc.* **1972**, *94*, 2552-2553. DOI: https://doi.org/10.1021/ja00762a082

(62) Charpin, P.; Marquet-Ellis, H.; Folcher, G. Uranium(IV) borohydride: A new crystalline form. *J. Inorg. Nucl. Chem.* **1979**, *41*, 1143-1144. DOI: https://doi.org/10.1016/0022-1902(79)80472-8

(63) Charpin, P.; Nierlich, M.; Vigner, D.; Lance, M.; Baudry, D. Structure of the second crystalline form of uranium(IV) tetrahydroborate. *Acta Crystallogr. C* **1987**, *43*, 1465-1467. DOI: https://doi.org/10.1107/S0108270187091431

(64) Schlesinger, H. I.; Brown, H. C. Uranium(IV) Borohydride. *J. Am. Chem. Soc.* **1953**, *75*, 219-221. DOI: https://doi.org/10.1021/ja01097a058

(65) Fazakerley, G. V.; Folcher, G.; Marquet-Ellis, H. Dissociation of uranium(III) and uranium(IV) borohydrides in solution: ^{11}B, ^{1}H NMR study. *Polyhedron* **1984**, *3*, 457-461. DOI: https://doi.org/10.1016/S0277-5387(00)84518-0

(66) Marks, T. J.; Kolb, J. R. Covalent transition metal, lanthanide, and actinide tetrahydroborate complexes. *Chem. Rev.* **1977**, *77*, 263-293. DOI: https://doi.org/10.1021/cr60306a004

(67) Cotton, F. A.; Daniels, L. M.; Murillo, C. A.; Wang, X. *nido*-Metalloborane Complexes: Synthesis and Structural Characterization of μ_2,η^4-Hexahydrodiboratotetrakis(*N*,*N*'-diarylformamidinato)ditantalum(III), Aryl = p-Tolyl and Phenyl. The First Structurally Characterized Complexes Containing the μ_2,η^4-$B_2H_6^{2-}$ Ligand. *J. Am. Chem. Soc.* **1996**, *118*, 4830-4833. DOI: https://doi.org/10.1021/ja954087d

(68) Ting, C.; Messerle, L. Borohydride boron-hydrogen activation and dimerization by a doubly bonded, early-transition-metal organodimetallic complex. Ditantalladiborane syntheses as models for dehydrodimerization of methane to ethane. *J. Am. Chem. Soc.* **1989**, *111*, 3449-3450. DOI: https://doi.org/10.1021/ja00191a063

(69) Aldridge, S.; Shang, M.; Fehlner, T. P. Synthesis of Novel Molybdaboranes from (η^5-C_5R_5)$MoCl_n$ Precursors (R = H, Me; n = 1, 2, 4). *J. Am. Chem. Soc.* **1998**, *120*, 2586-2598. DOI: https://doi.org/10.1021/ja973720n

(70) Cabon, N.; Pétillon, F. Y.; Schollhammer, P.; Talarmin, J.; Muir, K. W. Reaction of BH_4^- with {Mo_2Cp_2(μ-SMe)} species to give tetrahydroborato, hydrido or dimetallaborane compounds: control of product by ancillary ligands. *Dalton Trans.* **2004**, 2708-2719. DOI: https://doi.org/10.1039/B407564A

(71) Brunner, H.; Gehart, G.; Meier, W.; Wachter, J.; Wrackmeyer, B.; Nuber, B.; Ziegler, M. L. Präparative, ^{11}B-, ^{93}Nb-NMR-spektroskopische und strukturelle Untersuchungen an Cp_2NbBH_4 und $[CpNb(B_2H_6)]^{2-}$Komplexen. *J. Organomet. Chem.* **1992**, *436*, 313-324. DOI: https://doi.org/10.1016/0022-328X(92)85063-3

(72) Ghosh, S.; Beatty, A. M.; Fehlner, T. P. The Reaction of Cp*ReH_6, Cp* = C_5Me_5, with Monoborane to Yield a Novel Rhenaborane. Synthesis and Characterization of

arachno-Cp*$ReH_3B_3H_8$. *Collection of Czechoslovak Chemical Communications* **2002**, *67*, 808-812. DOI: https://doi.org/10.1135/cccc20020808

(73) Bose, S. K.; Geetharani, K.; Ramkumar, V.; Mobin, S. M.; Ghosh, S. Fine Tuning of Metallaborane Geometries: Chemistry of Metallaboranes of Early Transition Metals Derived from Metal Halides and Monoborane Reagents. *Chem. Eur. J.* **2009**, *15*, 13483-13490. DOI: https://doi.org/10.1002/chem.200901819

(74) Bose, S. K.; Geetharani, K.; Ramkumar, V.; Varghese, B.; Ghosh, S. Chemistry of Vanadaboranes: Synthesis, Structures, and Characterization of Organovanadium Sulfide Clusters with Disulfido Linkage. *Inorg. Chem.* **2010**, *49*, 2881-2888. DOI: https://doi.org/10.1021/ic9023597

(75) *SHAPE 2.1: Program for the Stereochemical Analysis of Molecular Fragments by Means of Continuous Shape Measures and Assosciated Tools*; 2013. http://www.ee.ub.edu.

(76) Pyykkö, P. Additive Covalent Radii for Single-, Double-, and Triple-Bonded Molecules and Tetrahedrally Bonded Crystals: A Summary. *J. Phys. Chem. A* **2015**, *119*, 2326-2337. DOI: https://doi.org/10.1021/jp5065819

(77) Leverd, P. C.; Lance, M.; Vigner, J.; Nierlich, M.; Ephritikhine, M. Synthesis and reactions of uranium(IV) tetrathiolate complexes. *J. Chem. Soc., Dalton Trans.* **1995**, 237-244. DOI: https://doi.org/10.1039/DT9950000237

(78) Falcone, M.; Chatelain, L.; Mazzanti, M. Nucleophilic Reactivity of a Nitride-Bridged Diuranium(IV) Complex: CO_2 and CS_2 Functionalization. *Angew. Chem., Int. Ed.* **2016**, *55*, 4074-4078. DOI: https://doi.org/10.1002/anie.201600158

(79) Groom, C. R.; Bruno, I. J.; Lightfoot, M. P.; Ward, S. C. The Cambridge Structural Database. *Acta Crystallogr. B* **2016**, *72*, 171-179. DOI: https://doi.org/10.1107/S2052520616003954

(80) Bubrin, D.; Niemeyer, M. Isostructural Potassium and Thallium Salts of Sterically Crowded Thio- and Selenophenols: A Structural and Computational Study. *Eur. J. Inorg. Chem.* **2008**, *2008*, 5609-5616. DOI: https://doi.org/10.1002/ejic.200800756

(81) Windorff, C. J.; Cross, J. N.; Scott, B. L.; Kozimor, S. A.; Evans, W. J. Crystallographic characterization of $(C_5H_4SiMe_3)_3U(BH_4)$. *Acta Crystallogr. E* **2021**, *77*, 383-389. DOI: https://doi.org/10.1107/S2056989021002425

(82) Adam, R.; Villiers, C.; Ephritikhine, M.; Lance, M.; Nierlich, M.; Vigner, J. Reactions of ketones with uranium tetraborohydride, mechanism and stereoselectivity, synthesis and structure of uranium (IV) tetrahydroborato alkoxide complexes. *New J. Chem.* **1993**, 455-464. DOI: https://www.osti.gov/etdeweb/biblio/6077406

(83) Blake, P. C.; Lappert, M. F.; Taylor, R. G.; Atwood, J. L.; Hunter, W. E.; Zhang, H. Synthesis, spectroscopic properties and crystal structures of $[ML_2Cl_2]$[M = Th or U; L =η-$C_5H_3(SiMe_3)_2$-1,3] and $[UL_2X_2]$(X = Br, I or BH_4). *J. Chem. Soc., Dalton Trans.* **1995**, 3335-3341. DOI: https://doi.org/10.1039/DT9950003335

(84) Scott, P.; Hitchcock, P. B. Exploring the auxiliary co-ordination sphere of tripodal amino(triamido) actinide complexes. *J. Chem. Soc., Dalton Trans.* **1995**, 603-609. DOI: https://doi.org/10.1039/DT9950000603

(85) Baudry, D.; Bulot, E.; Charpin, P.; Ephritikhine, M.; Lance, M.; Nierlich, M.; Vigner, J. Pentadienyluranium borohydride complexes and their cyclopentadienyl analogues; crystal structures of (η-2,4-$Me_2C_5H_5$)$U(BH_4)_3$ and (η-C_5H_5)$U(BH_4)_3$. *J. Organomet. Chem.* **1989**, *371*, 163-174. DOI: https://doi.org/10.1016/0022-328X(89)88023-4

(86) Rebizant, J.; Spirlet, M. R.; Bettonville, S.; Goffart, J. Structure of bis[(1,2,3,3a,7a-η)-indenyl]bis(tetrahydroborato)uranium(IV). *Acta Crystallogr. C* **1989**, *45*, 1509-1511. DOI: https://doi.org/10.1107/S0108270189001940

(87) Rietz, R. R.; Edelstein, N. M.; Ruben, H. W.; Templeton, D. H.; Zalkin, A. Preparation and crystal structure of uranium(IV) borohydride-bis(tetrahydrofuran),

$U(BH_4)_4 \cdot 20C_4H_8$. *Inorg. Chem.* **1978**, *17*, 658-660. DOI: https://doi.org/10.1021/ic50181a029

(88) Charpin, P.; Nierlich, M.; Vigner, D.; Lance, M.; Baudry, D. Structure of (tetrahydroborato)bis(tetrahydrofuran)uranium(IV): a model for hydrogen-uranium bonding. *Acta Crystallogr. C* **1987**, *43*, 1630-1631. DOI: https://doi.org/10.1107/S0108270187090814

(89) Müller, M.; Williams, V. C.; Doerrer, L. H.; Leech, M. A.; Mason, S. A.; Green, M. L. H.; Prout, K. Syntheses of the Uranium Complexes $[U\{N(SiMe_3)_2\}_2\{N(SiMe_3)(SiMe_2CH_2B(C_6F_5)_3)\}]$ and $[U\{C(Ph)(NSiMe_3)_2\}_2\{\mu^3\text{-}BH_4\}_2]$. Determination of Hydrogen Positions by Single-Crystal X-ray and Neutron Diffraction. *Inorg. Chem.* **1998**, *37*, 1315-1323. DOI: https://doi.org/10.1021/ic970891k

(90) Arliguie, T.; Baudry, D.; Ephritikhine, M.; Nierlich, M.; Lance, M.; Vigner, J. Synthesis, crystal structure and dynamic behaviour in solution of monocyclooctatetraene uranium alkoxides. *J. Chem. Soc., Dalton Trans.* **1992**, 1019-1024. DOI: https://doi.org/10.1039/DT9920001019

(91) Baudin, C.; Baudry, D.; Ephritikhine, M.; Lance, M.; Navaza, A.; Nierlich, M.; Vigner, J. Influence of electronic factors on the structure and stability of uranium compounds. Tri-tert-butyl methoxide uranium(IV) complexes. *J. Organomet. Chem.* **1991**, *415*, 59-73. DOI: https://doi.org/10.1016/0022-328X(91)83281-8

(92) Baudry, D.; Bulot, E.; Ephritikhine, M.; Nierlich, M.; Lance, M.; Vigner, J. Monocyclooctatetraenyluranium(IV) borohydrides. Crystal structure of $(\eta\text{-}C_8H_8)U(BH_4)_2(OPPh_3)$. *J. Organomet. Chem.* **1990**, *388*, 279-287. DOI: https://doi.org/10.1016/0022-328X(90)85375-9

(93) Arliguie, T.; Blug, M.; Le Floch, P.; Mézailles, N.; Thuéry, P.; Ephritikhine, M. Organouranium Complexes with Phosphinine-Based SPS Pincer Ligands. Variations

with the Substituent at the Phosphorus Atom. *Organometallics* **2008**, *27*, 4158-4165. DOI: https://doi.org/10.1021/om8003493

(94) Zalkin, A.; Rietz, R. R.; Templeton, D. H.; Edelstein, N. M. Preparation and crystal structure of uranium(IV) borohydride-n-propyl ether. *Inorg. Chem.* **1978**, *17*, 661-663. DOI: https://doi.org/10.1021/ic50181a030

(95) Charpin, P.; Nierlich, M.; Chevrier, G.; Vigner, D.; Lance, M.; Baudry, D. Structure du complexe bis(oxyde de triphenylphosphine)tetrakis(tetrahydroborato)uranium(IV). *Acta Crystallogr. C* **1987**, *43*, 1255-1258. DOI: https://doi.org/10.1107/S0108270187092242

(96) Baudry, D.; Charpin, P.; Ephritikhine, M.; Lance, M.; Nierlich, M.; Vigner, J. Synthesis of a uranium (IV) hydride from the corresponding borohydride: preparation of $\{(MeOCH_2CH_2OMe)U(BH_4)_3(\mu\text{-}H)\}_2$ and the crystal structure of its toluene solvate. *J. Chem. Soc., Chem. Commun.* **1987**, 739-740. DOI: https://doi.org/10.1039/C39870000739

(97) Cantat, T.; Arliguie, T.; Noël, A.; Thuéry, P.; Ephritikhine, M.; Floch, P. L.; Mézailles, N. The U═C Double Bond: Synthesis and Study of Uranium Nucleophilic Carbene Complexes. *J. Am. Chem. Soc.* **2009**, *131*, 963-972. DOI: https://doi.org/10.1021/ja807282s

(98) Charpin, P.; Lance, M.; Soulie, E.; Vigner, D.; Marquet-Ellis, H. Structure du complexe bis(oxyde de triphenylphosphine)tetrakis(tetrahydroborato)uranium(IV) solvate avec le benzene. *Acta Crystallogr. C* **1985**, *41*, 1723-1726. DOI: https://doi.org/10.1107/S0108270185009210

(99) Baudry, D.; Charpin, P.; Ephritikhine, M.; Folcher, G.; Lambard, J.; Lance, M.; Nierlich, M.; Vigner, J. Synthesis and crystal structure of the volatile monocyclopentadienyl uranium complex $(\eta\text{-}C_5H_5)U(BH_4)_3$. *J. Chem. Soc., Chem. Commun.* **1985**, 1553-1554. DOI: https://doi.org/10.1039/C39850001553

(100) Arnold, P. L.; Farnaby, J. H.; Gardiner, M. G.; Love, J. B. Uranium(III) Coordination Chemistry and Oxidation in a Flexible Small-Cavity Macrocycle. *Organometallics* **2015**, *34*, 2114-2117. DOI: https://doi.org/10.1021/om5012193

(101) Zanella, P.; De Paoli, G.; Bombieri, G.; Zanotti, G.; Rossi, R. A new uranium(IV) organometallic tetrahydroborate complex. The preparation and characterization of the bis(cyclopentadienyl)uranium (iv) bis(tetrahydroborate):(η^5-$C_5H_5)_2U(BH_4)_2$. *J. Organomet. Chem.* **1977**, *142*, C21-C24. DOI: https://doi.org/10.1016/S0022-328X(00)94350-X

(102) Wasserman, H. J.; Moody, D. C.; Paine, R. T.; Ryan, R. R.; Salazar, K. V. Tetrahydroborate complexes of uranium with 2-(diphenylphosphino)pyridine. *J. Chem. Soc., Chem. Commun.* **1984**, 533-534. DOI: https://doi.org/10.1039/C39840000533

(103) Rietz, R. R.; Zalkin, A.; Templeton, D. H.; Edelstein, N. M.; Templeton, L. K. Preparation and molecular and crystal structures of uranium(IV) borohydride-dimethyl ether and uranium(IV) borohydride-diethyl ether. *Inorg. Chem.* **1978**, *17*, 653-658. DOI: https://doi.org/10.1021/ic50181a028

(104) Shannon, R. D. Revised effective ionic radii and systematic studies of interatomic distances in halides and chalcogenides. *Acta Crystallogr. A* **1976**, *32*, 751-767. DOI: https://doi.org/10.1107/s0567739476001551

(105) Kar, S.; Kar, K.; Bairagi, S.; Bhattacharyya, M.; Chowdhury, M. G.; Ghosh, S. Chalcogen stabilized borate complexes of tantalum. *Inorg. Chim. Acta* **2022**, *530*, 120685. DOI: https://doi.org/10.1016/j.ica.2021.120685

(106) Huang, Y.; Stephan, D. W. Reductions of Cyclopentadienyltitanium Diolate and Dithiolate Species with Boron and Tin Hydrides. *Organometallics* **1995**, *14*, 2835-2842. DOI: https://doi.org/10.1021/om00006a032

(107) Bianchini, C.; Masi, D.; Meli, A.; Peruzzini, M.; Vizza, F.; Zanobini, F. C−S Bond Cleavage of Benzo[*b*]thiophene at Ruthenium. *Organometallics* **1998**, *17*, 2495-2502. DOI: https://doi.org/10.1021/om980051t

(108) Ramalakshmi, R.; Saha, K.; Roy, D. K.; Varghese, B.; Phukan, A. K.; Ghosh, S. New Routes to a Series of σ-Borane/Borate Complexes of Molybdenum and Ruthenium. *Chem. Eur. J.* **2015**, *21*, 17191-17195. DOI: https://doi.org/10.1002/chem.201503404

(109) Song, H.; Ye, K.; Geng, P.; Han, X.; Liao, R.; Tung, C.-H.; Wang, W. Activation of Epoxides by a Cooperative Iron–Thiolate Catalyst: Intermediacy of Ferrous Alkoxides in Catalytic Hydroboration. *ACS Catalysis* **2017**, *7*, 7709-7717. DOI: https://doi.org/10.1021/acscatal.7b02527

(110) Khasnis, D. V.; Pirio, N.; Touchard, D.; Toupet, L.; Dixneuf, P. H. Activation of dithioformate by iron complexes: insertion of alkynes into the coordinated C-S bond. X-ray structures of Fe[η^3-H-B(H)2←S-C(SMe)H](CO)(PMe_3)$_2$ and Fe[η^3-S-C(Ph)=CH-CH(SMe)](CO)(PMe_3)$_2$. *Inorg. Chim. Acta* **1992**, *198-200*, 193-201. DOI: https://doi.org/10.1016/S0020-1693(00)92361-2

(111) Sellmann, D.; Hille, A.; Heinemann, F. W.; Moll, M.; Reiher, M.; Hess, B. A.; Bauer, W. Binding H_2, N_2, H^-, and BH_3 to Transition-Metal Sulfur Sites: Synthesis and Properties of [Ru(L)(PR_3)('$N_2Me_2S_2$')] Complexes (L=η^2-H_2, H^-, BH_3; R=Cy, *i*Pr). *Chem. Eur. J.* **2004**, *10*, 4214-4224. DOI: https://doi.org/10.1002/chem.200400120

(112) Muetterties, E. L. *nido*-Metalloboranes. *Pure Appl. Chem.* **1972**, *29*, 585-596. DOI: https://doi.org/10.1351/pac197229040585

(113) CCDC 249351: Experimental Crystal Structure Determination.

(114) Franz, D.; Szilvási, T.; Pöthig, A.; Deiser, F.; Inoue, S. Three-Coordinate Boron(III) and Diboron(II) Dications. *Chem. Eur. J.* **2018**, *24*, 4283-4288. DOI: https://doi.org/10.1002/chem.201800609

(115) Morss, L. R.; Edelstein, N. M.; Fuger, J. *The Chemistry of the Actinide and Transactinide Elements*; Springer Dordrecht, 2011. DOI: https://doi.org/10.1007/978-94-007-0211-0.

(116) Clifton, J. R.; Gruen, D. M.; Ron, A. Electronic Absorption Spectra of Matrix‐Isolated Uranium Tetrachloride and Uranium Tetrabromide Molecules. *J. Chem. Phys.* **1969**, *51*, 224-232. DOI: https://doi.org/10.1063/1.1671711

(117) Auzel, F.; Hubert, S.; Delamoye, P. Absolute oscillator strengths of 5f-5f transitions of U^{4+} in $ThBr_4$ and in hydrobromic acid solutions. *J. Lumin.* **1982**, *26*, 251-262. DOI: https://doi.org/10.1016/0022-2313(82)90053-9

(118) Carnall, W. T.; Liu, G. K.; Williams, C. W.; Reid, M. F. Analysis of the crystal‐field spectra of the actinide tetrafluorides. I. UF_4, NpF_4, and PuF_4. *J. Chem. Phys.* **1991**, *95*, 7194-7203. DOI: https://doi.org/10.1063/1.461396

(119) Kindra, D. R.; Evans, W. J. Magnetic susceptibility of uranium complexes. *Chem. Rev.* **2014**, *114*, 8865-8882. DOI: https://doi.org/10.1021/cr500242w

(120) Seed, J. A.; Birnoschi, L.; Lu, E.; Tuna, F.; Wooles, A. J.; Chilton, N. F.; Liddle, S. T. Anomalous magnetism of uranium(IV)-oxo and -imido complexes reveals unusual doubly degenerate electronic ground states. *Chem* **2021**, *7*, 1666-1680. DOI: https://doi.org/10.1016/j.chempr.2021.05.001

(121) Réant, B. L. L.; Berryman, V. E. J.; Seed, J. A.; Basford, A. R.; Formanuik, A.; Wooles, A. J.; Kaltsoyannis, N.; Liddle, S. T.; Mills, D. P. Polarised covalent thorium(IV)– and uranium(IV)–silicon bonds. *Chem. Commun.* **2020**, *56*, 12620-12623. DOI: https://doi.org/10.1039/D0CC06044E

(122) van Leusen, J.; Speldrich, M.; Kögerler, P. Magnetism of Actinide Coordination Compounds. In *Organometallic Magnets*, Chandrasekhar, V., Pointillart, F. Eds.; Springer International Publishing, 2018; pp 391-410.

(123) Moro, F.; Mills, D. P.; Liddle, S. T.; van Slageren, J. The inherent single-molecule magnet character of trivalent uranium. *Angew. Chem., Int. Ed.* **2013**, *52*, 3430-3433. DOI: https://doi.org/10.1002/anie.201208015

(124) Bart, S. C.; Heinemann, F. W.; Anthon, C.; Hauser, C.; Meyer, K. A New Tripodal Ligand System with Steric and Electronic Modularity for Uranium Coordination Chemistry. *Inorg. Chem.* **2009**, *48*, 9419-9426. DOI: https://doi.org/10.1021/ic9012697

(125) Dan, X.; Du, J.; Zhang, S.; Seed, J. A.; Perfetti, M.; Tuna, F.; Wooles, A. J.; Liddle, S. T. Arene-, Chlorido-, and Imido-Uranium Bis- and Tris(boryloxide) Complexes. *Inorg. Chem.* **2024**. DOI: https://doi.org/10.1021/acs.inorgchem.3c04275

(126) Neese, F. Software update: The ORCA program system—Version 5.0. *WIRES Comput. Mol. Sci.* **2022**, *12*, e1606. DOI: https://doi.org/10.1002/wcms.1606

(127) Perdew, J. P.; Ernzerhof, M.; Burke, K. Rationale for mixing exact exchange with density functional approximations. *J. Chem. Phys.* **1996**, *105*, 9982-9985. DOI: https://doi.org/10.1063/1.472933

(128) Adamo, C.; Barone, V. Toward reliable density functional methods without adjustable parameters: The PBE0 model. *J. Chem. Phys.* **1999**, *110*, 6158-6170. DOI: https://doi.org/10.1063/1.478522

(129) Bader, R. F. W.; Matta, C. F. Atomic Charges Are Measurable Quantum Expectation Values: A Rebuttal of Criticisms of QTAIM Charges. *J. Phys. Chem. A* **2004**, *108*, 8385-8394. DOI: https://doi.org/10.1021/jp0482666

(130) Davidson, E. R.; Clark, A. E. A viewpoint on population analyses. *Int. J. Quant. Chem.* **2022**, *122*, e26860. DOI: https://doi.org/10.1002/qua.26860

(131) North, S. C.; Jorgensen, K. R.; Pricetolstoy, J.; Wilson, A. K. Population analysis and the effects of Gaussian basis set quality and quantum mechanical approach: main

group through heavy element species. *Frontiers in Chemistry* **2023**, *11*. DOI: https://doi.org/10.3389/fchem.2023.1152500

(132) Cho, M.; Sylvetsky, N.; Eshafi, S.; Santra, G.; Efremenko, I.; Martin, J. M. L. The Atomic Partial Charges Arboretum: Trying to See the Forest for the Trees. *ChemPhysChem* **2020**, *21*, 688-696. DOI: https://doi.org/10.1002/cphc.202000040

(133) Price, A. N.; Berryman, V.; Ochiai, T.; Shephard, J. J.; Parsons, S.; Kaltsoyannis, N.; Arnold, P. L. Contrasting behaviour under pressure reveals the reasons for pyramidalization in tris(amido)uranium(III) and tris(arylthiolate) uranium(III) molecules. *Nat. Commun.* **2022**, *13*, 3931. DOI: https://doi.org/10.1038/s41467-022-31550-7

(134) Deng, C.; Liang, J.; Sun, R.; Wang, Y.; Fu, P.-X.; Wang, B.-W.; Gao, S.; Huang, W. Accessing five oxidation states of uranium in a retained ligand framework. *Nat. Commun.* **2023**, *14*, 4657. DOI: https://doi.org/10.1038/s41467-023-40403-w

(135) Keerthi Shivaraam, R. A.; Keener, M.; Modder, D. K.; Rajeshkumar, T.; Zivkovic, I.; Scopelliti, R.; Maron, L.; Mazzanti, M. A Route to Stabilize Uranium(II) and Uranium(I) Synthons in Multimetallic Complexes. *Angew. Chem., Int. Ed.* **2023**, *62*, e202304051. DOI: https://doi.org/10.1002/anie.202304051

(136) Cryer, J. D.; Liddle, S. T. 4.08 - Arene Complexes of the Actinides. In *Comprehensive Organometallic Chemistry IV*, Parkin, G., Meyer, K., O'Hare, D. Eds.; Elsevier, 2022; pp 460-501.

(137) Van der Sluys, W. G.; Burns, C. J.; Huffman, J. C.; Sattelberger, A. P. Uranium alkoxide chemistry. 1. Synthesis and the novel dimeric structure of the first homoleptic uranium(III) aryloxide complex. *J. Am. Chem. Soc.* **1988**, *110*, 5924-5925. DOI: https://doi.org/10.1021/ja00225a067

(138) Liddle, S. T. Inverted sandwich arene complexes of uranium. *Coord. Chem. Rev.* **2015**, *293-294*, 211-227. DOI: https://doi.org/10.1016/j.ccr.2014.09.011

(139) Arnold, P. L.; Halliday, C. J. V.; Puig-Urrea, L.; Nichol, G. S. Instantaneous and Phosphine-Catalyzed Arene Binding and Reduction by U(III) Complexes. *Inorg. Chem.* **2021**, *60*, 4162-4170. DOI: https://doi.org/10.1021/acs.inorgchem.1c00327

(140) Lam, F. Y. T.; Wells, J. A. L.; Ochiai, T.; Halliday, C. J. V.; McCabe, K. N.; Maron, L.; Arnold, P. L. A Combined Experimental and Theoretical Investigation of Arene-Supported Actinide and Ytterbium Tetraphenolate Complexes. *Inorg. Chem.* **2022**, *61*, 4581-4591. DOI: https://doi.org/10.1021/acs.inorgchem.1c03365

(141) Wooles, A. J.; Mills, D. P.; Tuna, F.; McInnes, E. J. L.; Law, G. T. W.; Fuller, A. J.; Kremer, F.; Ridgway, M.; Lewis, W.; Gagliardi, L.; Vlaisavljevich, B.; Liddle, S. T. Uranium(III)-carbon multiple bonding supported by arene δ-bonding in mixed-valence hexauranium nanometre-scale rings. *Nat. Commun.* **2018**, *9*, 2097. DOI: https://doi.org/10.1038/s41467-018-04560-7

(142) Hadlington, T. J.; Hermann, M.; Li, J.; Frenking, G.; Jones, C. Activation of H_2 by a Multiply Bonded Amido–Digermyne: Evidence for the Formation of a Hydrido–Germylene. *Angew. Chem., Int. Ed.* **2013**, *52*, 10199-10203. DOI: https://doi.org/10.1002/anie.201305689

(143) Wright, R. J.; Brynda, M.; Power, P. P. Synthesis and Structure of the “Dialuminyne” $Na_2[Ar'AlAlAr']$ and $Na_2[(Ar''Al)_3]$: Al–Al Bonding in Al–Na– and Al–Na– Clusters. *Angew. Chem., Int. Ed.* **2006**, *45*, 5953-5956. DOI: https://doi.org/10.1002/anie.200601925

(144) Bursten, B. E.; Palmer, E. J.; Sonnenberg, J. L. On the Role of *f*-Orbitals in the Bonding in *f*-Element Complexes: the “Feudal” Model as Applied to Organoactinide and Actinide Aquo Complexes. In *Recent Advances In Actinide Science*, Alvares, R., Bryan, N. D., May, I. Eds.; Special Publications, The Royal Society of Chemistry, 2006; pp 157-162.